PONTIFICIA UNIVERSIDAD CATÓLICA DE CHILE
ESCUELA DE INGENIERÍA

MODELING PRESENT AND FUTURE CONDITIONS OF ANTARCTIC LAKES ICE COVERS

SEBASTIÁN IGNACIO ECHEVERRÍA ALAR

Thesis submitted to the Office of Research and Graduate Studies
in partial fulfillment of the requirements for the degree of
Master of Science in Engineering

Advisor:
FRANCISCO SUÁREZ POCH

Santiago de Chile, December 2017

PONTIFICIA UNIVERSIDAD CATÓLICA DE CHILE
ESCUELA DE INGENIERÍA

MODELING PRESENT AND FUTURE CONDITIONS OF ANTARCTIC LAKES ICE COVERS

SEBASTIÁN IGNACIO ECHEVERRÍA ALAR

Members of the Committee:
FRANCISCO SUÁREZ POCH
SARAH LERAY
ALBERTO DE LA FUENTE STRANGER
NICOLÁS BAMBACH
ENZO SAUMA SANTIS

Thesis submitted to the Office of Research and Graduate Studies
in partial fulfillment of the requirements for the degree of
Master of Science in Engineering

Santiago de Chile, December 2017

To Julia.

ACKNOWLEDGEMENTS

First, I would like to thank my thesis advisor; Dr. Francisco Suárez Poch, for all his support, encouragement, time, suggestions and concern to carry out this investigation. In this way I learned, for the first time, what is teamwork. I'll be eternally grateful.

I would also like to thank Nicolás Bambach for all his time and help whenever I needed. With our conversations, I was able to land several concepts and applied them to this work. Alike, I would like to thank to Sebastián Vicuña for all his advices in climate change projections. I would also like to thank Mark Hausner, who gave me various advices to make this study as robust as possible. I want to make a special thanks to Maciej Obryk, who without knowing me answered my mails to discuss about his work, and handed me data that I couldn't have gotten otherwise. I would also like to thank the Comisión Nacional de Investigación Científica y Tecnológica (CONICYT), Chile, for funding project Fondecyt N°1170850, which allowed me to participate in the 2017 American Geophysical Union Fall Meeting.

I would also like to thank to my brother, father and mother (and Bruno) for being the most important company I had during this process, and for their unconditional love. I hope that with this pages, they finally understand what I did in these two and a half years. I would also like to thank to my aunt Patricia for her kindness and concern.

I would also like to thank to my friends from Antofagasta, without you guys everything would have been different (probably I would have finished this thesis faster). I would also thank to my college friends for teaching me that it is possible to create new bonds in a small period of time.

Finally, but not less important, I would like to thank to the person who appeared at the end of this phase; Magdalena. You arrived to fill with colors my mind, an you gave me more reasons to finish this work. This is also for you. Thank you.

TABLE OF CONTENTS

LIST OF FIGURES

LIST OF TABLES

RESUMEN

Los lagos Antárticos son excelentes indicadores del cambio climático, ya que se encuentran en una región aislada donde el impacto humano y animal es despreciable. En este estudio, un modelo 1-D para lagos con cubierta de hielo fue implementado y validado, para después investigar el impacto de cambio climático sobre las cubiertas de hielo de dos lagos Antárticos: el lóbulo oeste del Lago Bonney (WLB) y el Lago Crooked. El modelo es forzado por los flujos de radiación, los flujos atmosféricos, y por el flujo de calor turbulento proveniente del cuerpo de agua bajo la cubierta de hielo. Los resultados del modelo coinciden bien con los espesores de hielo medidos en ambos lagos, y fueron razonables con las mediciones de ablación en WLB. Las diferencias entre la ablación medida y la modelada se deben a que el modelo consider la variabilidad interanual de las propiedades ópticas del hielo ni los cambios estacionales en la estructura térmica del lago. Los resultados muestran que hacia fines de este siglo, la cubierta de hielo de WLB seguirá siendo perenne, aún cuando a partir del $\sim$2050 las altas temperaturas de verano aumentarán considerablemente el derretimiento de la cubierta. En el Lago Crooked la cubierta de hielo dejará de ser perenne debido a que hacia fines de este siglo, la temperatura del aire estará por aproximadamente un tercio del año.

Palabras Claves: Lagos Antárticos con cubierta de hielo, modelamiento de hielo, cambio climático.

ABSTRACT

Antarctic lakes are excellent indicators of climate variability as they are in an isolated region where human and animal impact are negligible. In this study, a 1-D ice-lake model was implemented and validated, to then investigate the impact of climate change on the ice covers from two Antarctic lakes: West Lake Bonney (WLB) and Crooked Lake. The model is forced by radiative fluxes, atmospheric fluxes, and the turbulent heat flux from the water body beneath the ice cover. Model results agreed well with measured ice thickness of both lakes (WLB - RMSE=0.11 m over 16 years of data; Crooked Lake - RMSE=0.07 m over 1 year of data), and had acceptable results with measured ablation data at WLB (RMSE=0.28 m over 6 years). The differences between the measured and modeled ablation occurred because the model did not take into account the the interannual variability of the ice optical properties, and the seasonal changes of the thermal structure from the lake. Results show that by the end of this century, the ice cover of WLB will remain perennial, even when from $\sim$2050 the forecasted high summer air temperatures will increase the ice-cover melting. By the end of the century at Crooked Lake the ice cover will not be perennial because the air temperatures will be above freezing for about one third of the year.

Keywords: Antarctic ice-covered lakes, ice modeling, climate change.

1. CONTEXT

Projections of climate change scenarios are needed to understand how ecosystems will respond in the future (Reid & Crout, 2008). However, it is difficult to engage this problem because of the great uncertainty associated to the climate itself, and to the global circulation models used today (Kay et al., 2015). The uncertainty of the models is strongly connected with all the parametrizations and assumptions of biological, chemical and physical processes that occurs in the atmosphere, the land, the ocean, and the cryosphere (Kay et al., 2015; Lenaerts, Vizcaino, Fyke, van Kampenhout, & van den Broeke, 2016). Therefore, it is necessary to develop tools that allows to comprehend climate change with less uncertainty as possible.

To reduce this uncertainty it is fundamental to choose a study site with enough and accessible meteorological information and that is known for responding to changes in climate. Places with such features are lakes. They are well known as sentinels of climate change as many of their physical, chemical and biological properties are sensitive to variations in meteorological and hydrological conditions (Laird, Fritz, Grimm, & Mueller, 1996; Oviatt, 1997; Benson et al., 1998; Schindler, 2009; Williamson, Saros, Vincent, & Smol, 2009; Adrian et al., 2009; Schindler, 2009; Castendyk, Obryk, Leidman, Gooseff, & Hawes, 2016). Further in endorheic basins, lakes are the lowest points of watersheds; linking the climate processes effects across landscapes (Castendyk et al., 2016), being this integration characteristic for this type of lakes (LaBaugh et al., 1997). Polar and sub-polar lakes are considered some of the most sensitive lakes to climate change (W. F. Vincent, Laurion, & Pienitz, 1998; Lyons, Laybourn-Parry, Welch, & Priscu, 2006; A. C. Vincent, Mueller, & Vincent, 2008; Adrian et al., 2009; Williamson et al., 2009; Paquette, Fortier, Mueller, Sarrazzin, & Vincent, 2015; Castendyk et al., 2016). In particular, perennially ice-covered, meromictic antarctic lakes are exceptional candidates to be indicators of climate variability and change as a result of their isolation from direct human and animal impact (Wharton Jr. et al., 1992; Fountain et al., 1999; Smith, 1999; W. F. Vincent et al., 1998; Reid & Crout, 2008).

For example, the McMurdo Dry Valleys (MDV) of Victoria Land, Antarctica, is a place that contains several ice-covered lakes with these features, and is distinctly sensitive to climate variations as small perturbations can lead to extreme variations in the hydrologic regime; also known as polar amplification phenomena (Dana, Wharton Jr., & Dubayah, 1998; Fountain, Dana, Lewis, Vaughn, & McKnight, 1998; Fountain et al., 1999). Another Antarctic place with lakes of such characteristics is Vestfold Hills of Princess Elizabeth Land. In fact, it has the largest concentration of meromictic lakes in Antarctica, and possibly in the whole world (Burke & Burton, 1988; Gallagher, Burton, & Calf, 1989; Gibson, 1999). Lakes at Vestfold Hills are generally saline or hypersaline near the coast, and fresh near the Antarctic Plateau (Burke & Burton, 1988).

Mathematical models are useful tools to understand how these ice-covered lakes respond to climate forcing. Several models have been used to solve the thermodynamics of ice shelves and covers. Since the classical analytical model proposed by Stefan (1891), many computational models of different complexity have been developed (e.g., Maykut & Untersteiner, 1971; Semtner, 1976; Launiainen & Cheng, 1998; Bitz & Lipscomb, 1999; Reid & Crout, 2008; Hunke, Lipscomb, Turner, Jeffery, & Elliot, 2015; Obryk, Doran, Hicks, McKay, & Priscu, 2016). Hunke et al. (2015) developed the Los Alamos Sea Ice Model (CICE), which is an open-source code that solves the thermodynamics of ice shelves considering radiative, conductive and turbulent heat fluxes, among other physical processes. The model implemented in the present study is based on the work of Reid & Crout (2008), and on CICE with the aim of investigating the impact of climate change on the ice cover. The details of the model and its assumptions are described later in this document.

1.1. Hypothesis

The hypothesis of this work is that the application of a sea-ice model in an ice-covered lake allows to quantify the existing thermodynamic interactions between atmosphere-ice cover-lake, and to evaluate the response of this system to climate change.

1.2. Objectives

The general objective of this study is to quantify the temporal evolution of the ice covers from two Antarctic lakes: WLB and Crooked Lake; and to analyze their future behavior under different climate deltas. The specific objectives of this thesis are: 1) to obtain the necessary measurements of meteorological data and optical properties of ice for each lake, to use them as input data in the ice model; 2) to choose a global circulation model, to get future projection outputs for their later use to simulate the response of the ice covers under climate change conditions; and 3) to validate the implemented model with the available ice thickness data from each lake.

1.3. Structure of the thesis

To achieve these objectives, Section 1 introduces the importance of lakes as climate change indicators and Section 2 describes WLB and Crooked Lake. In Section 3, the methodology used in this study is explained, and details of the input and validation data are given. Section 4 shows the validation results of both lakes, and the temporal evolution of the two ice covers under three future hybrid climate deltas. In Section 5, these results are discussed and compared to previous studies in both sites. Finally, in Section 6 conclusions are shown, highlighting the importance of having a lake-ice model to understand the ice cover dynamics of these lakes.

2. INTRODUCTION

Lakes are well known as sentinels of climate change as many of their physical, chemical and biological properties are sensitive to variations in meteorological and hydrological conditions (Laird et al., 1996; Oviatt, 1997; Benson et al., 1998; Schindler, 2009; Williamson et al., 2009; Adrian et al., 2009; Schindler, 2009; Castendyk et al., 2016). Further in endorheic basins, lakes are the lowest points of watersheds; linking the climate processes effects across landscapes (Castendyk et al., 2016), being this integration characteristic for this type of lakes (LaBaugh et al., 1997). Polar and sub-polar lakes are considered some of the most sensitive lakes to climate change (W. F. Vincent et al., 1998; Lyons et al., 2006; A. C. Vincent et al., 2008; Adrian et al., 2009; Williamson et al., 2009; Paquette et al., 2015; Castendyk et al., 2016). In particular, perennially ice-covered, meromictic antarctic lakes are exceptional candidates to be indicators of climate variability and change as a result of their isolation from direct human and animal impact (Wharton Jr. et al., 1992; Fountain et al., 1999; Smith, 1999; W. F. Vincent et al., 1998; Reid & Crout, 2008).

The McMurdo Dry Valleys (MDV) of Victoria Land, Antarctica (Figure 1.1a), is a place that contains several lakes with these features, and is distinctly sensitive to climate variations as small perturbations can lead to extreme variations in the hydrologic regime; also known as polar amplification phenomena (Dana et al., 1998; Fountain et al., 1998, 1999). This site was discovered by Sir Robert Falcon Scott (Scott, 1905), who made observations of lake levels and their ice covers. Nowadays, large meteorological and physical data of different lakes exists thanks to the expeditions made by the New Zealand Antarctic Program, and the United States, McMurdo Dry Valleys, Long Term Ecological Research (MCM-LTER) Program (Castendyk et al., 2016).

The lakes of the MDV have been studied over 80 years. Specifically, the features of Lakes Bonney, Fryxell, Hoare and Vanda have been widely recorded (Spigel & Priscu, 1998; Gibson, 1999). Ragotzkie & Likens (1964) studied Lakes Bonney and Vanda, noting

their different albedo and thermal structures, establishing the basis of how distinctive the lakes within MDV can be. With meteorological information collected between 1986 and 2000, Doran et al. (2002) made a climate analysis of the MDV. They investigated the behavior of Taylor (Figure 2.1a), Wright, and Victora Valleys. They found that Lake Vanda, located in Wright Valley, was the warmest place in summer with 74.7 degree days above freezing in average, whereas Lake Brownworth, also in Wright Valley, was the coldest site in summer with only 6.2 degree days above freezing in average. Castendyk et al. (2016) discussed the changes to the physical characteristics of Lake Vanda, mainly the loss of ice cover and rise of the lake level. They showed that the reason of ice thinning in this lake was the warming of the shallow water, and the lake level rise was closely related to the regional climate change, which increases air temperatures and the frequency of foehn winds. Obryk et al. (2016) studied the evolution of the ice covers of Lakes Bonney and Fryxell. They associated the long-term trends of the ice thickness not only to climate change, but also to the thermal structure of each lake. They found that the lake deep heat storage, speeds up or retards the response of ice covers to climate changes.

Recently, Gooseff et al. (2017) investigated the impact of an unusual austral summer (2001-2002) on physical and biological properties of perennial ice-covered lakes from the MDV. In this season, the maximum mean air temperature ($\sim$3 °C) coincided with one of the highest mean summer solar fluxes recorded ($\sim$242 W m^{-2}). Thus, a decadal summer cooling phase (-1.2 °C per decade) ended suddenly in 2002 provoking the greatest amount of glacial meltwater since 1969. This singular period was named 'flood year' by the authors. As a consequence the perennial ice covers began to thin significantly until today. For example, the ice cover of the west lobe of Lake Bonney (WLB), located in Taylor Valley (Figure 2.1a), thickenned from 1987 to 2001 at a rate of 0.85 m per decade, and since 2002 it began to thin at a rate of 0.61 m per decade (Gooseff et al., 2017). These results showed that it is likely that long-term changes of ice thickness are linked to abrupt events in response to climate change.

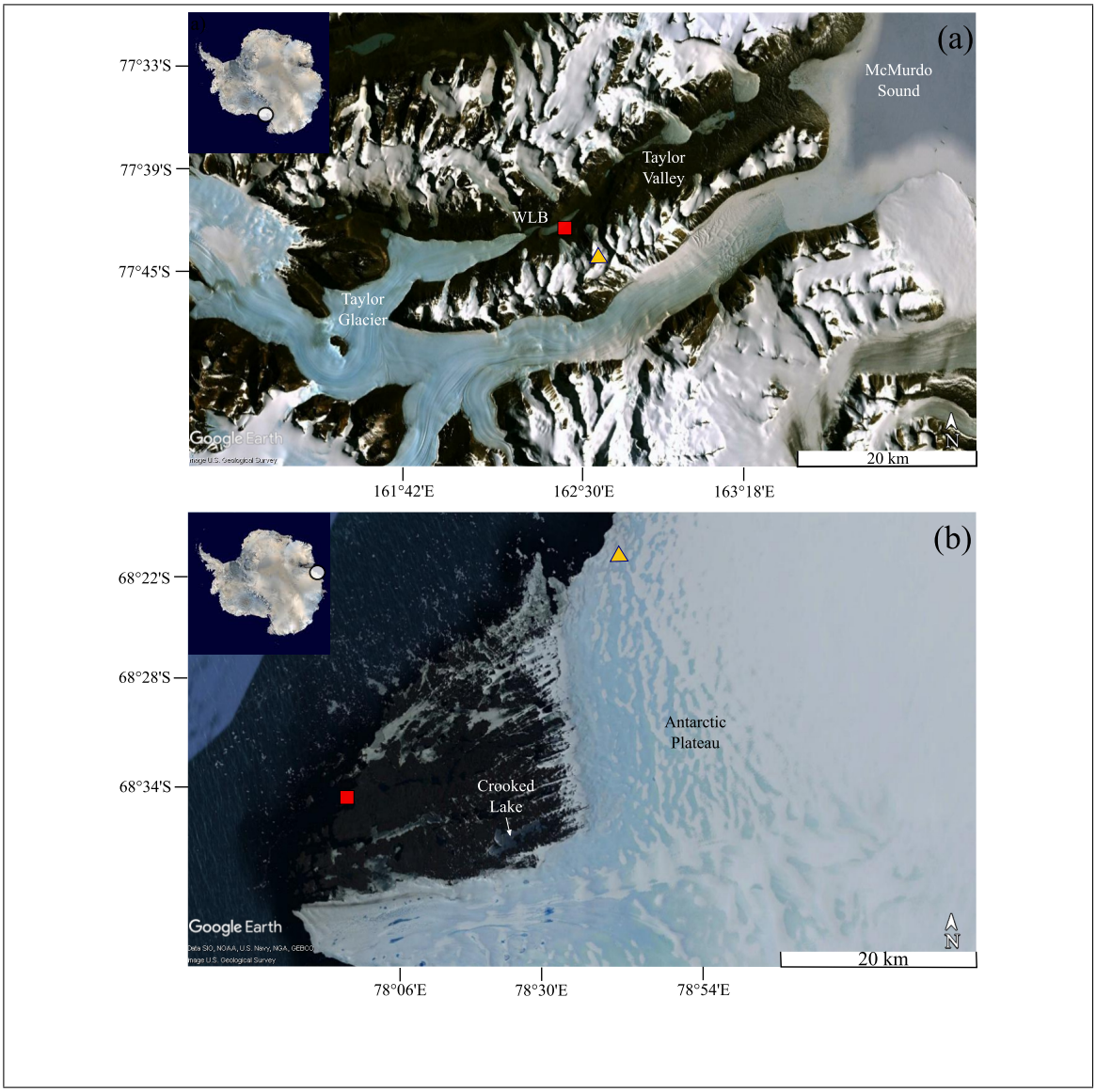

Figure 2.1. (a) Map from a portion of the MDV, showing WLB (Taylor Valley); the McMurdo Sound; and the Taylor Glacier, which is an outer glacier from the Antarctic Plateau. (b) Map of Vestfold Hills indicating the position of Crooked Lake. Squares represents the location of the meteorological stations, and triangles defines the centroids of the global cells, from the climatological models, used in the simulations of each lake.

Another Antarctic place with lakes of such characteristics is Vestfold Hills of Princess Elizabeth Land. In fact, it has the largest concentration of meromictic lakes in Antarctica, and possibly in the whole world (Burke & Burton, 1988; Gallagher et al., 1989; Gibson,

1999). Lakes at Vestfold Hills are generally saline or hypersaline near the coast, and fresh, as Crooked Lake (Figure 2.1b), near the Antarctic Plateau (Burke & Burton, 1988). In 2003, insights of the ice cover seasonal behavior from Crooked Lake were found by Reid & Crout (2008). They established that in such lake, the water temperature was affected mainly by air temperature changes.

In this work, we analyze if changes in climate can lead to substantial responses of Antarctic ice-covered lakes. To accomplish this objective,an ice-lake model was developed and validated. Then, air temperature projections from the Community Earth System Model-Large Ensemble (CESM-LE) under a business-as-usual scenario (RCP8.5) were used to simulate the evolution of the ice covers of WLB and Crooked Lake under climate change. The aim of choosing these particular lakes was to show insights on how climate change will affect Antarctic ice covers with distinct meteorological forcing, physical properties, and lake thermal structure.

3. SITES DESCRIPTION

This study focuses on two Antarctic lakes: WLB, and Crooked Lake. WLB is located in Taylor Valley of the MDV, as shown in Figure 2.1a. Crooked Lake is situated in Vestfold Hills (Figure 2.1b).

The MDV of Victoria Land, Antarctica are ice-free terrains with perennially ice-covered lakes supplied by glacial melt (Ragotzkie & Likens, 1964; Fountain et al., 1999; Doran et al., 2002; Castendyk et al., 2016; Obryk et al., 2016). Additionally, the MDV are within a polar desert, where mean annual temperatures range from -14.8 to -30.0 °C, and the precipitation rate is less than 50 mm year^{-1} (Doran et al., 2002; Fountain, Nylen, Monaghan, Basagic, & Bromwich, 2010; Castendyk et al., 2016).The interannual variability of their ice covers ranged between 3 and 6 m over the past two decades (Obryk et al., 2016). Lake Bonney ($77^\circ\ 44'$ S, $161^\circ\ 10'$ E) lies at the lowest part of the MDV (Hoare et al., 1964; Doran et al., 2002). It is influenced by strong, warm and dry katabatic winds from the Polar Plateau (Doran et al., 2002; Obryk et al., 2016). Doran et al. (2002) determined that Lake Bonney is the second warmest site (during summer) in the MDV, having on average 34.3 degree days above freezing between 1993-2000.

The Vestfold Hills of Princess Elizabeth Land, Antarctica, similarly than the MDV, are ice-free terrains (Gibson, 1999). An important difference with the MDV is that some lakes of this place may lose their ice cover for a brief period during the austral summer (Laybourn-Parry & Pearce, 2007). Gibson (1999) observed that the ice covers from Vestfold Hills had ice thickness between 0.5 and 2 m. This area is also a polar desert, where mean annual temperatures range from -8.9 to -12.0 °C, and the precipitation rate is about 64.2 mm year^{-1} (Barnes-Keoghan, 2016). Crooked Lake ($68^\circ\ 37'$ S, $78^\circ\ 22.3'$ E) is one of the largest ($\sim$12.6 km^2) and deepest (140 m) freshwater lakes in Antarctica (Gibson, 1999; Reid & Crout, 2008). It is, in particular, affected by strong katabatic winds from the Antarctic Plateau (Reid & Crout, 2008). Crooked Lake had on average 43.3 degree days above freezing on the period 1996-2003 (Barnes-Keoghan, 2016).

4. MATERIALS AND METHODS

4.1. Model description

Several models have been used to solve the thermodynamics of ice shelves. Since the classical analytical model proposed by Stefan (1891), many computational models of different complexity have been developed (e.g., Maykut & Untersteiner, 1971; Semtner, 1976; Launiainen & Cheng, 1998; Bitz & Lipscomb, 1999; Reid & Crout, 2008; Hunke et al., 2015; Obryk et al., 2016). Hunke et al. (2015) developed the Los Alamos Sea Ice Model (CICE), which is an open-source code that solves the thermodynamics of ice shelves considering radiative, conductive and turbulent heat fluxes, among other physical processes. The model implemented in the present study is based on the work of Reid & Crout (2008), and on CICE with the following assumptions: (i) only the thermodynamic aspects of ice are taken into account since the ice covers studied here are stable (Hibler III, 1979; Lepparanta, 2015); (ii) the model does not account for the effects of salinity -at the bottom of the ice cover of WLB the salinity is nearly zero, and Crooked Lake is a freshwater lake (Ragotzkie & Likens, 1964; McKay, Clow, Wharton, & Squyres, 1985; Reid & Crout, 2008); (iii) throughout the year there is no snow cover over the ice due to the low precipitation rates (Gibson, 1999; Fountain et al., 1999, 2010; Castendyk et al., 2016; Obryk et al., 2016); (iv) there is no lateral melting, even when melt ponds are created around the edges in the MDV lakes (Fountain et al., 1999). Nonetheless, they represent a small percentage of the total lake surface (Spigel & Priscu, 1998; Dugan, Obryk, & Doran, 2013); and (v) the incoming radiative fluxes are calculated based on equations of an Antarctic site (Reid & Crout, 2008; Obryk et al., 2016).

The model solves the 1-D heat transfer equation along the vertical direction considering heat conduction within the ice:

$$\frac{\partial}{\partial t}\left(\rho_i c_i T_i\left(z,t\right)\right) = \frac{\partial}{\partial z}\left(k_i \frac{\partial T_i\left(z,t\right)}{\partial z} - I(z,t)\right) \tag{4.1}$$

where z is the depth, t is the time, T_i is the ice temperature, ρ_i is the density of the ice, c_i is the specific heat capacity of ice, k_i is the thermal conductivity of ice and $I(z,t)$ is a heat source. The lateral heat conduction is neglected since the diffusion length scale in fresh ice is about 6 m in a year (Lepparanta, 2015). The term $I(z,t)$ is an internal heat source that represents the attenuation of the shortwave radiation that penetrates into the ice (Maykut & Untersteiner, 1971; Semtner, 1976), and it is modeled with the Beer-Lambert law (McKay et al., 1985; Obryk et al., 2016):

$$I(z,t) = \beta F_{sw} exp^{-\kappa z} \tag{4.2}$$

where β is the fraction of absorbed shortwave radiation that penetrates the ice (following Lepparanta (2015), this parameter was set to 0.45), F_{sw} is the shortwave radiation, and κ is the extinction coefficient.

The surface temperature (top boundary condition) is calculated from the ice-cover surface energy balance, which considers the radiative fluxes, the atmospheric turbulent fluxes, and the conductive heat flux at the top of the ice (Figure 4.1):

$$(1-\beta)(1-\alpha)F_{sw} + F_{lw\downarrow} - F_{lw\uparrow} + F_s + F_l = F_{ct} \tag{4.3}$$

where α is the albedo, $F_{lw\downarrow}$ is the incoming longwave radiation, $F_{lw\uparrow}$ is the outgoing longwave radiation, F_s is the sensible heat flux, F_l is the latent heat flux, and F_{ct} is the conductive heat flux at the top of the ice. The parameterization of all these fluxes is described in Appendix B. In this study, to determine the turbulent sensible and latent fluxes, the atmospheric stability is taken into account (Monin & Obukhov, 1954; Lumley & Panofsky, 1964; Launiainen & Cheng, 1998). The reader is referred to Appendix C for a detailed description of the turbulent boundary layer theory, which is used to estimate the sensible and latent heat fluxes in the present model. The melting rate at the top of the ice cover is modeled using Equation (4.4):

$$-\rho_i L_f \left[\frac{dh}{dt}\right]_{z=0} = \begin{cases} F_{net} - F_{ct} & if\ F_{net} > F_{ct} \\ 0 & otherwise \end{cases} \tag{4.4}$$

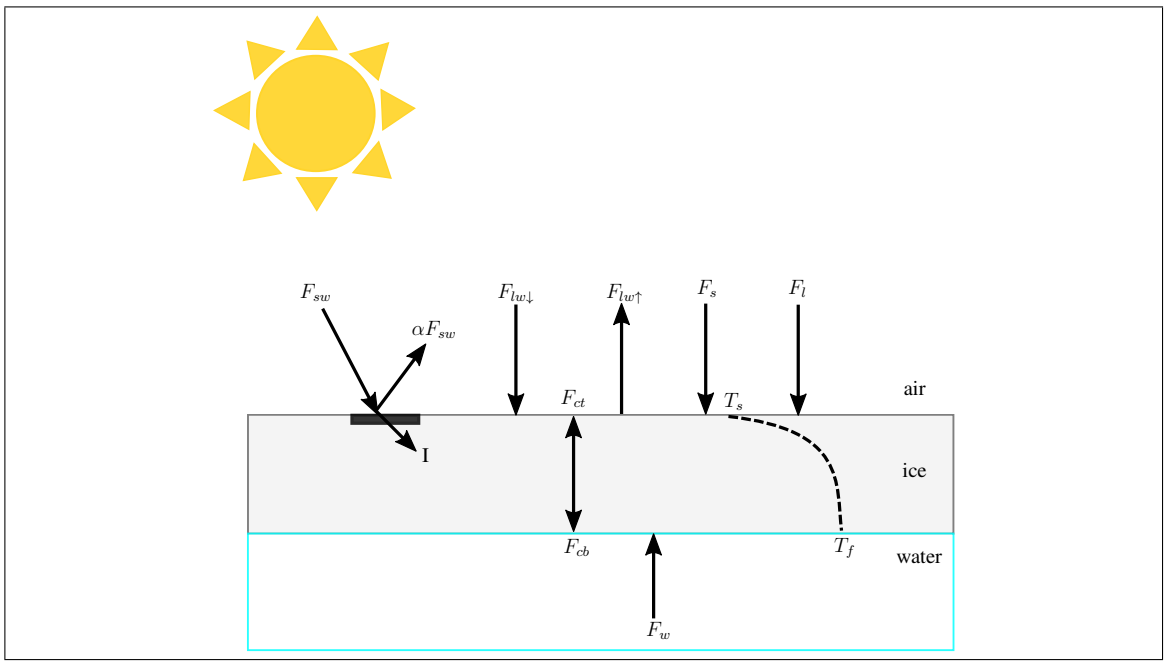

Figure 4.1. Schematic of heat fluxes on an ice-covered lake, and the temperature profile in the interior (dashed line). Fluxes toward the ice shelf are positive.

where h is the ice thickness of the top layer, L_f is the latent heat of freezing, and F_{net} is the net heat flux from the atmosphere (left side of Equation (4.3)). If the net heat flux from the atmosphere is greater than the conductive heat flux at the top of the ice, there is an excess of energy that will melt the top layer of the ice; otherwise, the ice thickness of the top layer remains constant. The model also takes into account the sublimation of the ice when latent heat is released to the atmosphere, according to what is proposed by Hunke et al. (2015):

$$-\rho_i \left(L_s - c_i T\right) \left[\frac{dh}{dt}\right]_{z=0} = F_l \tag{4.5}$$

where L_s is the latent heat of sublimation. Adding the rates of ice loss in Equations (4.4) and (4.5), the ablation rate at the top of the ice can be found. At the bottom of the ice cover, ice can grow or melt depending on the energy balance between the conductive heat flux that occurs at the bottom of the ice cover (F_{cb}) and the sensible heat flux from the lake (F_w), as shown in Figure 4.1. The rate of ice melt or growth at the bottom of the ice cover

is described by:

$$-\rho_i L_f \left[\frac{dh}{dt}\right]_{z=H} = F_{cb} + F_w \tag{4.6}$$

where h is the ice thickness of the bottom layer. The sensible heat at the ice-water interface, F_w, can be considered as a constant if its value is small (Maykut & Untersteiner, 1971), otherwise it should be modeled with the turbulent boundary layer theory as a bulk flux (see Appendix B.2.2 and Maykut & McPhee, 1995; Launiainen & Cheng, 1998; Reid & Crout, 2008).

Equations (4.1)-(4.6) were solved using the Backward Time-Centered Space (BTCS) implicit method, as it is a well known formulation to solve the 1-D heat equation (Kereyu & Gofe, 2016), coupled with the moving boundaries of the ice cover. In this way, the ice shelf was discretized into 50 equally spaced layers, where each one of them had a temperature that evolved in time. A 3-h time step was used in all the simulations. These discretizations were used following Reid & Crout (2008). The initial temperature profile of the ice was assumed to be linear between the surface temperature (being the initial one equal to the air temperature at the beginning of the simulation) and the fixed fresh water freezing temperature at the bottom (Reid & Crout, 2008; Obryk et al., 2016). Since some fluxes of Equation (4.3) depends on the surface temperature, this equation was solved using the iterative method described in Hunke et al. (2015). After the ice cover had melt or grow, the layers inside it did not have the same thicknesses anymore. To keep a uniform spatial discretization, the layers were updated based on the new value of the total ice thickness, H. Finally, to ensure energy conservation, the enthalpies of the new layers were recalculated (Hunke et al., 2015). A detailed description of the developed algorithm is given in Appendix D, and a flowchart of the model resolution in Appendix E.

4.2. Input data

The information needed to run the model are meteorological data: relative humidity, air temperature, wind speed, shortwave radiation (400-1100 nm), cloud cover; optical

properties of ice: albedo, extinction coefficient; and water temperature beneath the ice (or a known value of F_w).

For WLB the model was run with 16 years of information. The climate data were obtained from Lake Bonney's weather station (see Figure 2.1a for location) (Fountain & Doran, 2014). These data were sampled every 30 s, then averaged and stored every 15 min (Doran, Dana, Hastings, & Wharton, 1995; Doran et al., 2002). There is no information of cloud cover at Lake Bonney. Thus, in a similar way to that presented by Obryk et al. (2016), the cloud cover was defined as a random number with a uniform distribution generated at daily intervals. For details on the measurements of air temperature, wind speed and shortwave radiation the reader is referred to the work of Doran et al. (1995). The albedo was obtained from an interpolation based on 5 months (September-February) of the albedo measurements made by Fritsen & Priscu (1999). The generated albedo function was extrapolated to the rest of the year (spring and fall), to have an annual distribution. Because of the minor importance of shortwave radiation in spring and fall, and its absence in winter; the error associated to the extrapolation is considered to be small (Obryk et al., 2016). The extinction coefficient of ice was set to 0.85 (Howard-williams, Schwarz, Hawes, & Priscu, 1998). The sensible heat flux from the lake was considered as a constant, and was adjusted minimizing the RMSE between the modeled and measured values of ice thickness.

For Crooked Lake, the model was run with meteorological information of 2003. The climate data were recorded by the Australian Bureau of Meteorology staff at Davis Station every 3 h (see Figure 2.1b) (Reid & Crout, 2008); the water temperature of the lake and the optical properties of the ice were obtained with an automatic sensing probe every 5 min (see Palethorpe et al. (2004) for full understanding on how the parameters were measured).

Missing and flawed (thus removed) data existed at WLB because of failed sensors or failed dataloggers. In the case of air temperature, wind speed and relative humidity, the gaps were filled with daily averaged values based on the 16 years of data. For the case of

shortwave radiation, the missing values were obtained using the parametrization of Reid & Crout (2008) showed in Equation (B.1).

4.3. Validation data

Ice thickness of WLB were measured by Priscu (2014). The validation data contains measurements over 16 years, only in the austral summers (except in 2008 when data were recorded also during austral autumn) because of logistical restraints (Obryk et al., 2016). The ice thickness data were collected at drill hole sites within a 1000-m^2 grid, and in some days more than one measurement was made (in this case, ice thickness data were averaged). Also, continuous ablation data collected by Doran (2014) over 6 years were used to validate the model. These data were sampled every 1 min and then averaged over 20 min. The method to measure ablation is described by Dugan et al. (2013).

During 2003 in Crooked Lake, ice thickness data were sampled every 5 min and then averaged every 3 h using an automatic sensing probe (Palethorpe et al., 2004). However, between 1 February and 18 May a data gap exists because the ice cover was too thin to support the automatic sensing probe (Reid & Crout, 2008).

4.4. Climate projections

Future simulations were run using climatological information of the Community Earth System Model - Large Ensemble (CESM-LE) (Kay et al., 2015). CESM-LE considers 40 ensemble members, from 1920 to 2100 (except ensemble member 001, which starts from 1850), and a 2000+ year pre-industrial control run (Hurrel et al., 2013; Kay et al., 2015). The model couples the effects of an atmospheric model (CAM5; Gettelman et al., 2010), an ocean model (POP2; Smith et al., 2010), a land model (CLM4; Lawrence et al.,2011), and a sea ice model (CICE; Hunke et al.,2015). It also includes the effects of biogeochemistry and nitrogen limitation (Hurrel et al., 2013). The implementation of this sea ice component, showed improvements compared to earlier versions, influencing the

simulated climate feedbacks at high latitudes (Holland, Bailey, Briegleb, Light, & Hunke, 2012; Hurrel et al., 2013). The atmosphere and land grid set up resolution is $0.9^\circ \times 1.25^\circ$, while the resolution for the ocean and sea ice components is $\sim 1^\circ$ (Lenaerts et al., 2016).

The CESM-LE output used was the daily air temperature from all the ensemble members forced with a business-as-usual scenario of climate change; RCP8.5 (Meinshausen et al., 2009). As WLB and Crooked Lake are located in polar desert regions (Gibson, 1999; Castendyk et al., 2016; Obryk et al., 2016), changes in future precipitation rates were not analyzed. A hybrid delta approach, similar to that used by Hausner et al. (2016), was carried out considering the output from the 40 ensemble members, to generate the future air temperatures at both WLB and Crooked Lake. A difference was established between the observed and CESM-LE output daily air temperatures of the baseline period (1996-2011 for WLB, and 1996-2003 for Crooked Lake). For WLB, a moving average with a 16-years time frame was used, whereas at Crooked Lake the time frame was of 8 years, instead of 1 year (this was done to introduce more interannual variability to the air temperatures of this place). Daily air temperature data between 1996 and 2002 at Crooked Lake, were retrieved from the Australian Antarctic Data Centre (Barnes-Keoghan, 2016). Then, the 10^{th}, 50^{th}, and 90^{th} percentiles for the delta values were found, and they were applied to the daily averaged air temperatures of the baseline period, from the meteorological data of WLB and Crooked Lake, respectively. The outliers from the resulting time series were removed using a 3D phase space method (Goring & Nikora, 2002; Wahl, 2003; Mori, Suzuki, & Kakuno, 2007). These data were used to run the model towards the future. To evaluate the impact of climate change on the ice cover (thickness evolution, surface temperature, ablation, bottom melt and ice growth rates), three time periods were considered: historical (1996-2011 for WLB and only 2003 for Crooked Lake); mid-term (2040-2055); and long-term (2084-2099). The other meteorological data were averaged (the 16-years of information), with the purpose of obtaining a representative climate year of the historical period, and were used for future simulations at WLB, whereas at Crooked Lake future simulations were run with the same meteorological data from 2003, except the water temperature which, was determined as a function of the air temperature through the linear

regression proposed by Reid & Crout (2008). The optical properties of ice, in both lakes, were held constants.

4.5. Statistics for model evaluation

4.5.1. Nash-Sutcliffe coefficient of efficiency

To evaluate the performance of the proposed ice model, the Nash-Sutcliffe coefficient of efficiency (E) was used (Nash & Sutcliffe, 1970; Legates & McCabe Jr., 2005; Bennett et al., 2013). The E compares the efficacy of the model to a model that only uses the mean of the observed data (ice thickness in this case). It ranges from $-\infty$ to 1, in which the latter indicates the best agreement. A value of zero indicates that the performance is equally good if the mean observed data is used, while a value less than zero shows that the model prediction is worst than using the mean observed data. E is calculated as:

$$E = 1 - \frac{\sum_{i=1}^{n} (O_i - P_i)^2}{\sum_{i=1}^{n} \left(O_i - \bar{O}_i\right)} \tag{4.7}$$

where O_i are the observed (measured) data, $\bar{O}_i$ is the mean of the observed data, P_i are the predicted values from the model, and n is the number of data points used for the calculation.

4.5.2. Root mean square error

To evaluate the difference between the observed and modeled data, the root mean square error (RMSE) was used (Bennett et al., 2013):

$$\text{RMSE} = \sqrt{\frac{1}{n} \sum_{i=1}^{n} (O_i - P_i)^2} \tag{4.8}$$

4.5.3. Linear regressions

Linear regressions were found using the MATLAB function *regress*, which also report the coefficient of determination (r^2) and the p-value. In Section 5.2, future trends are calculated based on the median projected climate delta.

4.6. Sensitive analysis

A model sensitivity was performed by increasing or decreasing input parameters by 10% of their original values, except for air temperature, which was increased or decreased by 1 K. To evaluate the sensitivity, a simple sensitivity index (Si) was adopted from Hoffmann and Gardner (1983):

$$Si = \left| 1 - \frac{D_{min}}{D_{max}} \right| \tag{4.9}$$

where D_{min} is the model output (H) when a parameter was decreased, and D_{max} is the model output when the parameter was increased. Values closer to 1 indicates high sensitivity to changes, whereas Si <0.01 means no sensitivity to changes (Hoffmann & Gardner, 1983; Obryk et al., 2016).

5. RESULTS

5.1. Model validation

The ice model was validated with 16 years of measured ice thickness from WLB. For this lake there are no measurements of water temperature below the ice cover, so the sensible heat flux at the ice-water interface was adjusted by minimizing the RMSE between the modeled and measured ice thickness. Figure 5.1a shows three simulations of this adjustment: one considering F_w =3.5 W m^{-2}, other with F_w =5.5 W m^{-2}, and the last one considering F_w =7 W m^{-2}. These fluxes were held constant in the model because their values are small (Maykut & Untersteiner, 1971). Table 5.1 summarizes the statistical metrics of eight simulations with different values of F_w. The best fit was obtained when F_w =5.5 W m^{-2} with an RMSE of 0.21 m (see the red solid line in Figure 5.1a), and an E of 0.64.

Table 5.1. RMSE and E for all the modeled F_w at the ice-water interface.

F_w (W m^{-2})	3.5	4	4.5	5	5.5	6	6.5	7
RMSE (m)	0.7	0.53	0.38	0.27	0.21	0.24	0.32	0.41
E	-2.87	-1.24	-0.18	0.42	0.64	0.54	0.19	-0.36

Although the best fit was found with a constant value of F_w through the whole simulation (F_w =5.5 W m^{-2}), the trend of increasing ice thickness between 1996 and 2002 could not be predicted using a constant sensible heat flux. Therefore, we performed a second adjustment minimizing the RMSE of the sensible heat flux at the ice-water interface considering two periods divided by the day with the maximum ice thickness measured, i.e., from 1 January 1996 to 25 October 2001; and from 26 October 2001 to 1 January 2012. F_w at the first period was forced to be smaller, to obtain an increasing trend of ice thickness in this time lapse. Besides, as Gooseff et al. (2017) pointed out in their study,

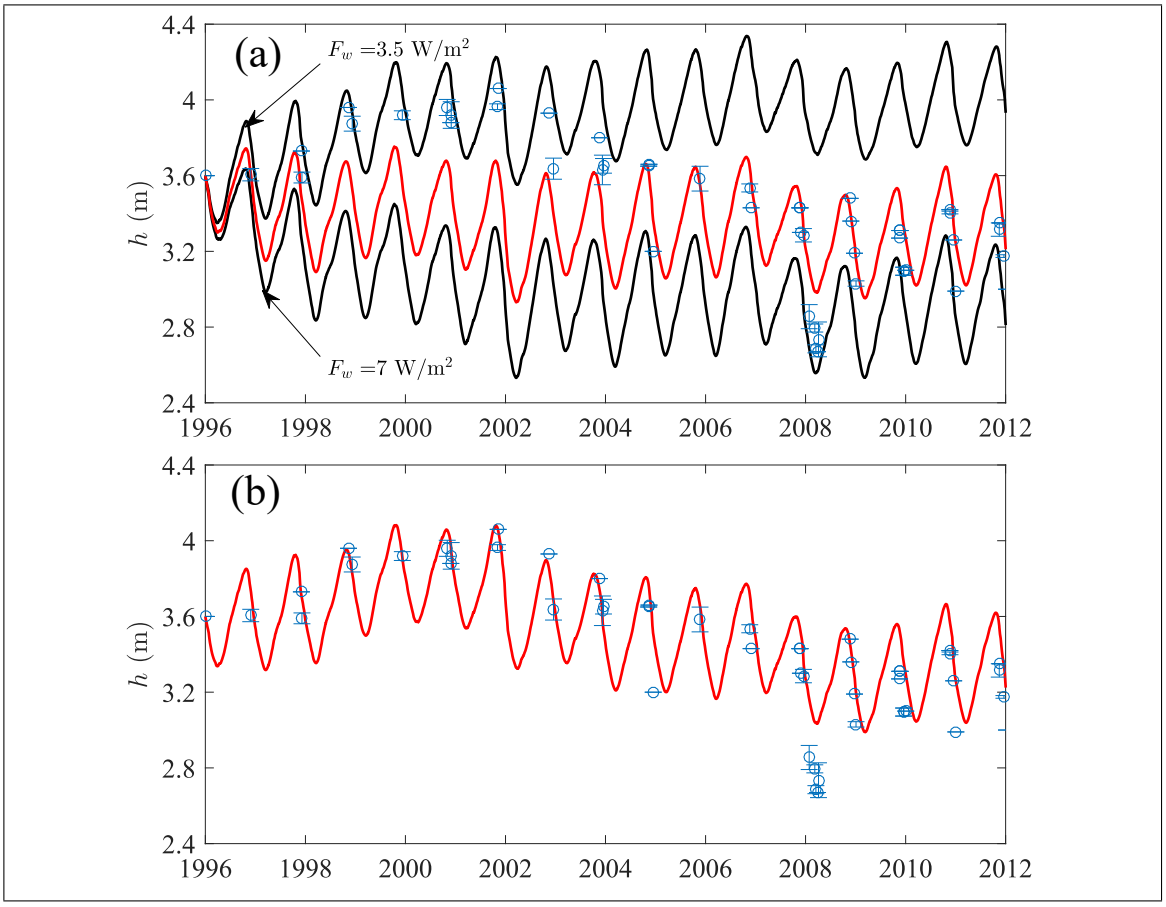

Figure 5.1. (a) Three simulations of the WLB ice cover evolution for 3.5 W m^{-2}< F_w <7.0 W m^{-2}. The circles correspond to the measured ice thicknesses and the red solid line is the best modeled ice thickness. The error bars represent the standard deviation of the ice thickness measurements. (b) Modeled ice thickness (solid line) forcing a change of the sensible heat flux at the ice bottom from October 26, 2001 until January 1, 2012. The drastic ice thinning in March 2008 could not be modeled. In that season, the ice was observed to be flooded with lake water. This indicates that seasonal variations of ice thickness, under specific conditions, cannot be well represented by the model.

in the austral summer of 2001-2002 a great amount of glacial meltwater was produced, which increased the stream flow into WLB. This meltwater episode thinned the perennial ice cover of WLB, most likely because a combination of the meteorological conditions and the changes in the sensible heat flux from the shallow water beneath the ice cover. The best adjustment was with F_w =3.8 W m^{-2} and F_w =5.9 W/m^2 for the best and second

time period, respectively. The latter value remained constant for the climate projections. The overall modeled ice thickness showed a better fitting to the data (Figure 5.1b) with an RMSE of 0.11 m, and an E of 0.87.

To complete the validation of WLB, the modeled ablation was compared with 6 years of measured ablation (Figure 5.2). A fit of r^2=0.96 (p<0.001) and an RMSE of 0.28 m were obtained. For an understanding on how the different parameters affected the ice thickness output, a sensitivity analysis was performed to the climate variables, optical properties of ice, F_{sw}, and F_w (considering the fitting case with two different values) in WLB. In Table 5.2 the sensitivity index (Si) is shown. Results suggest that ice thickness evolution is very sensitive to changes in solar radiation, and how it is absorbed and transmitted through the ice (optical properties). Also, the air temperature plays an important role in changes of ice thickness. Therefore, the variations on ice covers could reflect climate change. Ice thickness evolution is equally sensitive to the turbulent heat flux from the water body as to the air temperature. Thus, the long-term trends of ice thickness are affected by the heat below the ice cover (Obryk et al., 2016).

Table 5.2. Si values for the validation of 16 years in WLB.

F_{sw}	β	α	T_a	F_w	U_a	RH	C_s	C_l	κ
0.32	0.31	0.26	0.19	0.19	0.08	< 0.01	< 0.01	< 0.01	< 0.01

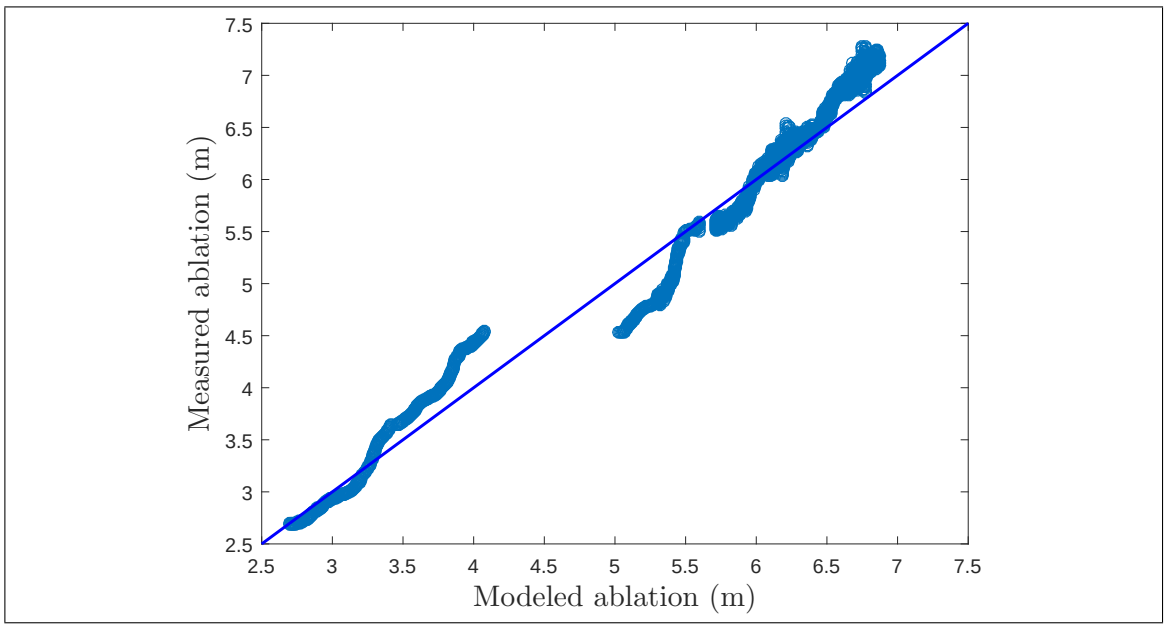

Figure 5.2. Comparison of the modeled and measured (over 6 years) ice ablation from WLB. Each data point represents 3 h averages. The 1:1 solid line is shown for comparison.

Also, the model was validated with the ice thickness measurements from Crooked Lake. Since this lake had data of water temperature below the ice cover, Equation (B.12) was used to model the sensible heat flux at the ice-water interface. Assuming a water speed of 1 mm/s (Reid & Crout, 2008), the bulk transfer coefficient, C_w, was adjusted (minimizing the RMSE as in WLB with F_w) obtaining a value of $3.9 \cdot 10^{-3}$ with an r^2 =0.94 ($p<0.001$) and an RMSE of 0.07 m (within the range of results found by Reid & Crout (2008); r^2=0.89 and an RMSE of 0.09 m). The modeled and averaged measured ice thickness for the year 2003 are shown in Figure 5.3. The model represented well the seasonal behavior of the ice cover within a year, although there is a data gap that occurred during the winter period. Model results predicted that the ice grew slower than the measured ice thickness, reaching a maximum modeled thickness that was slightly smaller than that observed. This behavior most likely occurred because the model did not consider seasonal variations on the surface of the ice; in winter the surface is smoother and flatter, and in summer it is broken and ridged (Reid & Crout, 2008). The incorporation of these features

would change the way of calculating the non-linear bulk transfer coefficients of the sensible and latent heat fluxes; affecting the sublimation rates, and the optical properties of the ice; affecting the melt rates at the surface.

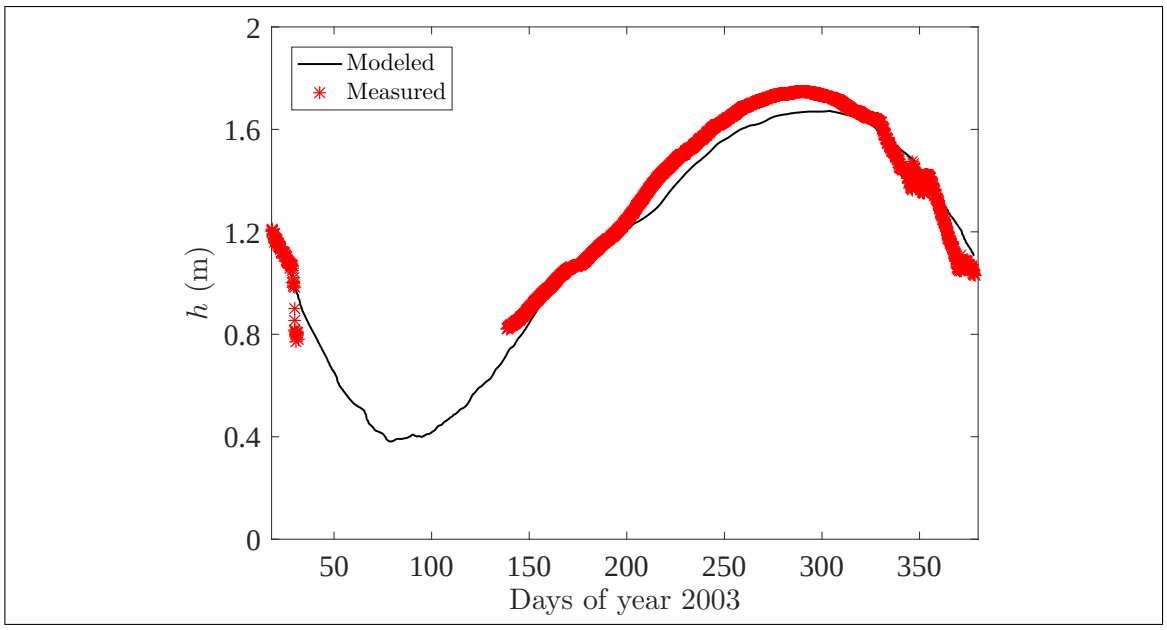

Figure 5.3. Modeled ice thickness and averaged (every 3 h) measured ice thickness by the automatic sensing probe from Crooked Lake.

5.2. Future projections of ice cover thicknesses

5.2.1. West Lake Bonney

Figure 5.4 shows the evolution of the mean annual ice thickness, the mean annual air temperature, and the mean summer air temperature between 1996 and 2099 at WLB. Under future climate conditions, the mean summer air temperatures at WLB rose at a rate of 0.52 °C per decade (p <0.001). Maximum mean air summer temperatures occurred in different years, and were different for each climate delta. The 2087-2088 austral summer, under the 90th percentile climate delta, was the warmest with a mean air temperature of -2.11 °C.

The ice cover of WLB exhibited different trends, during the future simulations. First, the ice thickened between the years 2012 and 2025 at a rate of 0.22 m per decade (p <0.001), reaching a maximum thickness of 3.66 m (under the 10th percentile climate delta). This thickness increase occurred because of the decrease in mean annual air temperatures between the historical and the first years of the future values. From 2025 to 2054 the ice cover thinned at a rate of 0.07 m per decade (p <0.001). Since 2054, each simulated climate delta surpassed the mean summer air temperature of the flood year described by Gooseff et al. (2017); and it could be thought as a new flood year, the ice cover thinned more quickly (0.19 m per decade; p <0.001) until 2098, dropping to a minimum of 2.34 m in the 90th percentile .

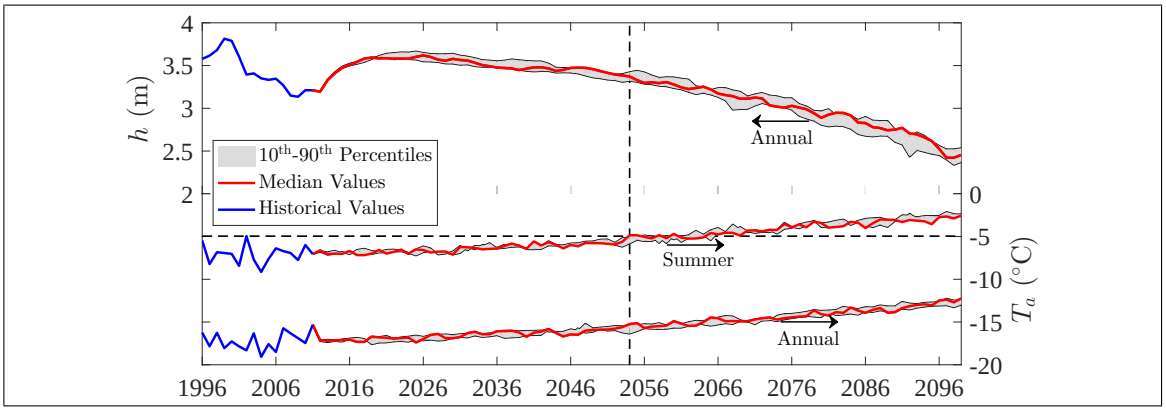

Figure 5.4. Time evolution of mean annual ice cover thickness, mean annual air temperature, and mean summer air temperature at WLB. Beginning in 2012, the three hybrid climate deltas (10th, 50th and 90th percentile climate deltas) of the CESM-LE output are shown. The black dashed lines indicates the year (2054) when the mean summer air temperatures will surpass the maximum mean summer air temperature of -4.95 °C that took place in the summer of the flood year.

Monthly average surface temperatures of the ice cover, and monthly ice thickness change rates in WLB, for each projected climate delta, are shown in Figure 5.5. For each climate delta, the ice surface temperature peaks occurred in December (coinciding with the peak of the ablation rates), and the temperature valleys occurred in August. Ablation

rates of the median projected climate delta decreased by approximately 0.86 cm per month in average between the historical and mid-term time periods, and they increased by about 1.52 cm per month in average between the mid- and long-term time periods. Conversely, bottom melt rates of the median projected climate delta rose by approximately 0.22 cm per month in average between the historical and mid-range time periods, and they stayed relatively constant between the mid- and long-term time periods. Among the present and mid-term time periods, the ice growth rates under the median projected climate delta decreased by 0.46 cm per month in average, and these rates increased to approximately 1.29 cm per month in average from the mid-term to the long-term time periods.

Historical and future simulations of mean total ice thickness change of the WLB ice cover; considering ablation, accretion, and bottom melt for each month, are summarized in Table 5.3. Results show that the ice cover lost ice every austral summer (January, February, March) and part of spring (November, December), peaking in December when ice surface temperature and ablation rates were higher (Figure 5.5). The exception is March, which exhibits an ice lost during the historical and mid-term perriods, but in the long-term period increases its thickness. This shift in ice cover loss was associated with the increase of ice growth rates between the mid and long-term time periods (Figure 5.5b, c). On the other hand, in autumn (April, May, June) and winter (July, August, September) the ice cover of WLB gained the majority of its ice, specially in midwinter (July, August).

Table 5.3. Monthly average total ice thickness change rate (cm month^{-1}) in WLB, defined as the ice growth minus the ablation and the bottom melt. To show interannual variability the monthly standard deviation is shown.

	Historical	Mid-term percentiles			Long-term percentiles		
Month		10th	50th	90th	10th	50th	90th
January	−13.6±2.5	−13.3±0.3	−13.3±0.2	−13.4±0.3	−15.9±1.6	−16.6±2.1	−16.7±1.9
February	−9±0.8	−9.4±0.2	−9.4±0.2	−9.4±0.2	−10.2±0.7	−10.1±0.4	−10.5±0.8
March	−1.1±1.6	−1.8±0.2	−1.8±0.3	−1.6±0.2	0.8±1.1	1.4±1.3	1.8±1
April	7.1±2.1	7.1±0.4	7.1±0.3	7.2±0.3	10.5±1.3	11±1.3	11.3±0.9
May	8.8±2.3	9.1±0.3	9.1±0.3	8.9±0.3	11.4±0.9	11.6±0.9	12±0.6
June	8.1±2	8.4±0.2	8.4±0.1	8.4±0.2	10.1±0.7	10.2±0.8	10.4±0.5
July	9±2	8.9±0.3	9.1±0.2	9.1±0.2	11.3±0.9	11.5±0.8	11.7±0.6
August	9.5±2	9.2±0.3	9.4±0.2	9.3±0.3	11±0.6	11.29±0.6	11.6±0.5
September	7.8±1.7	7.9±0.2	7.8±0.3	8±0.2	9.1±0.6	8.9±0.5	9.1±0.5
October	1.3±1.6	1±0.2	1.1±0.3	1.2±0.3	0.1±0.3	−0.2±0.5	−0.1±0.3
November	−13.3±3.1	−12.2±0.3	−12.4±0.3	−12.6±0.4	−15.6±2.4	−16±2.3	−16.1±1.7
December	−18.3±3.4	−16.1±0.7	−16.2±1.1	−16.3±0.9	−25.8±5.3	−27.2±3.9	−26.9±2.7

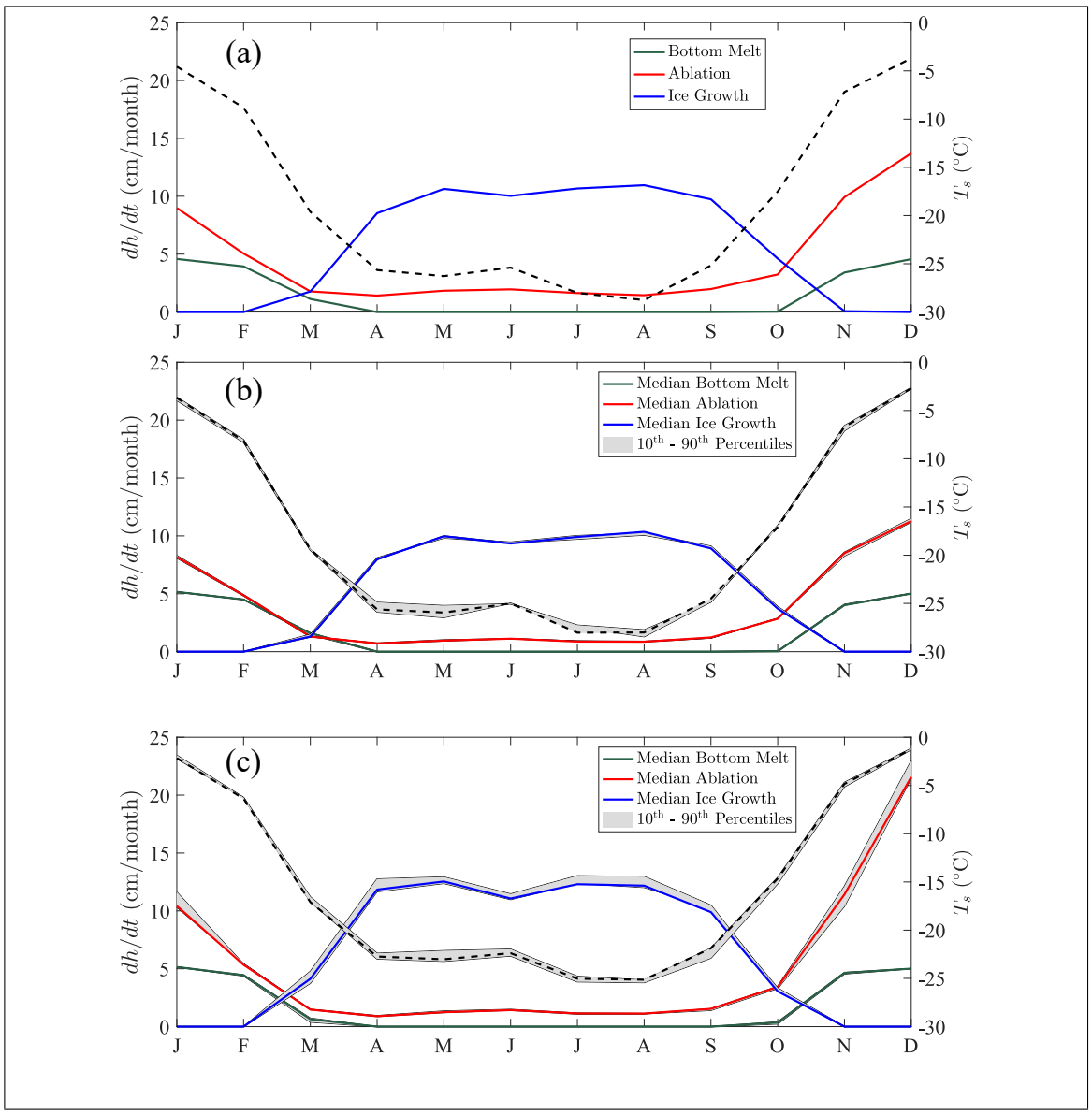

Figure 5.5. Monthly average simulated surface temperatures (black dashed line) and monthly cumulative ice thickness change rates in WLB. (a) Historical time period: 1996-2011. (b) Mid-term time period: 2040-2055. (c) Long-term time period: 2084-2099. The projected future periods shows the three hybrid climate deltas considering the 40 ensemble members from the CESM-LE.

5.2.2. Crooked Lake

Figure 5.6 shows the evolution of the mean annual ice thickness between 2003 and 2099; the evolution of the mean annual air temperature, and the mean summer air temperature between 1996 and 2099 at Crooked Lake. Under future CESM-LE simulations, the mean summer air temperatures at Crooked Lake rose at a rate of 0.47 °C per decade (p <0.001). Maximum mean air summer temperatures occurred in different years, and were different for each climate delta. The 2098-2099 austral summer, under the 50th percentile climate delta, was the warmest with a mean air temperature of 2.97 °C. This maximum temperature happened after the ice cover totally melted on 2069 when the mean summer air temperature was equal to 0.61 °C.

At Crooked Lake, the ice thinned at a rate of 0.07 m per decade (p <0.001) since 2004 until 2069 (under the 50th percentile climate delta), when the ice cover disappeared. The minimum ice thickness before 2069, was 0.89 m an occurred in 2068. The ice thickness evolution in Crooked Lake did not show an increase within the simulation period as in WLB. This was due to the low variability of the mean annual air temperatures for the historical period in Crooked Lake (see Figure 5.6), compared to those in WLB (standard deviations of 0.72 and 1.08 °C, respectively)

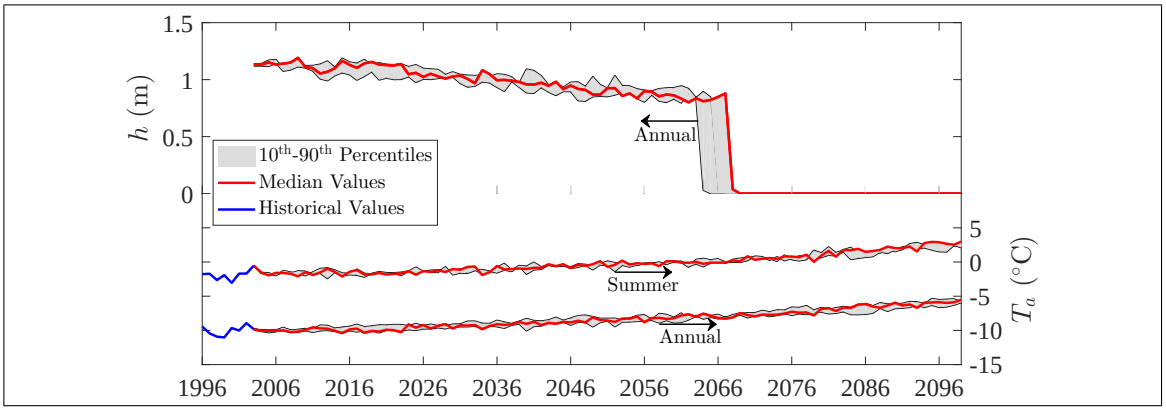

Figure 5.6. Time evolution of mean annual ice thickness cover, mean annual air temperature, and mean summer air temperature at Crooked Lake. Beginning in 2004, the three hybrid climate deltas (10^{th}, 50^{th} and 90^{th} percentile climate deltas) of the CESM-LE output are shown. The ice cover completely melts between the years 2064-2069. The historical mean annual ice thickness cover evolution is not shown as it only correspond to a 1-year period.

Monthly average surface temperatures of the ice cover, and monthly ice thickness change rates in Crooked Lake, for each projected climate delta, are shown in Figure 5.7. For each climate delta, in the mid-term simulations, the ice surface temperature peak occurred in January (coinciding with the peaks of the ablation and bottom melt rates), and the temperature valleys occurred in July. In the historical case, the maximum monthly average surface temperature occurred in December (the information from January was not found). Ablation rates of the median projected climate delta decreased by approximately 0.63 cm per month in average during February-December, between the historical and mid-term time periods . Similarly, bottom melt rates of the median projected climate delta decreased by approximately 1.33 cm per month in average during February-December, between the historical and mid-range time periods. Oppositely, within the present and mid-term time periods, the ice growth rates under the median projected climate delta increased by 1.93 cm per month in average in February-December. Comparisons with the long-term simulations are not presented because of the totally absence of ice.

Table 5.4. summarizes the historical and mid-term simulations of the mean total ice thickness change for each month in Crooked Lake. Results showed that this ice cover lost ice in part of austral summer (January, February) and every spring (October, November, December); including March of the historical simulation, peaking in January when ice surface temperature and ablation rates were higher (Figure 5.7). Steep changes in ice cover loss occurred in February and March, between the historical and mid-term time periods. These steep changes were related to the increase of ice growth rates among these periods (Figure 5.7a, b). Furthermore, in autumn (April, May, June) and winter (July, August, September) the ice cover in Crooked Lake gained the majority of its ice, with a maximum growth in May.

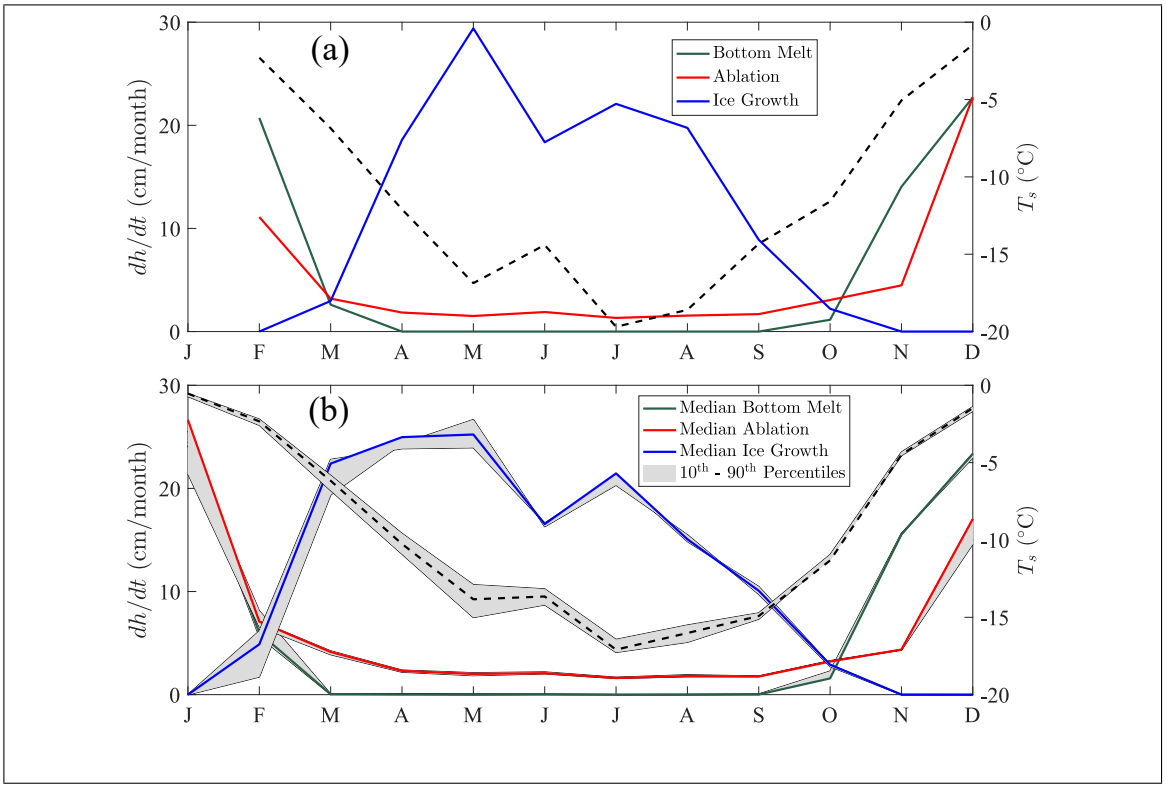

Figure 5.7. Monthly average simulated surface temperatures (black dashed line) and monthly cumulative ice thickness change rates in Crooked Lake. (a) Historical time period: 2003. There are no data for January owing to lack of information (the measurements of ice thickness began on 18 January). (b) Mid-term time period: 2040-2055, showing the three hybrid climate deltas. As the ice cover of Crooked Lake melted completely on 2065, the long-term time period is not included.

Table 5.4. Monthly average total ice thickness change rate (cm month^{-1}) in Crooked Lake, defined as the ice growth minus the ablation; and the bottom melt. To show interannual variability, the monthly standard deviation is also shown. As the historical data from Crooked Lake contemplates only 1-year period, its standard deviation is not shown. January has no data for the same reason mentioned above. Long-term simulations are not shown due to the lack of ice in that period.

	Historical	Mid-term percentiles		
Month		10th	50th	90th
January	-	–45.6±7	–51.2±5.9	–49.7±5.2
February	–31.8	–13±2.8	–8.2±3.9	–6.6±3.9
March	–2.8	15.4±4.2	18.2±3.2	18.5±3.2
April	16.8	22.1±3.1	22.7±2.4	21.4±2.3
May	27.9	24.8±3	23.2±3.3	21.8±1.8
June	16.5	14.2±3.1	14.4±2.2	14.4±3.3
July	20.8	18.7±3	19.9±2.5	19.5±3
August	18.2	13.7±2.1	13.3±4.1	12.9±2.5
September	7.2	7.9±3	8.3±1.6	8.7±2
October	–2	–2.8±1.7	–1.9±1.4	–2.3±1.6
November	–18.5	–20±2.5	–19.9±1.8	–19.9±2.2
December	–45.4	–37.6±2.8	–40.4±5	–40.4±3.7

6. DISCUSSION

Mean annual ice cover thickness of WLB responded to climate change temperatures under a RCP8.5 scenario dropping to a minimum of 2.34 m in the 90th percentile climate delta, on 2098, at a thinning rate of 0.19 m per decade. If the thinning continues at the same rate, ice cover of WLB will extinguish around the year 2220 becoming an ephemeral ice-covered lake for the first time in at least 320 years (Scott, 1905). In this way, WLB will be exposed to wind-driven turbulence, which will enhance mixing of the shallow water and may perturb the permanent vertical temperature stratification that exists nowadays (Hoare et al., 1964; Obryk et al., 2016). This effect, along with the change in absorbed radiation, most likely will modify primary production rates and phytoplankton dynamics (Fritsen & Priscu, 1999); forcing a total adaptation to the new WLB ecosystem. Nonetheless, these results must be considered carefully. For WLB, we adjusted F_w to represent in the best possible way the few available data of measured ice thickness. We obtained two fluxes; F_w =3.8 W m^{-2} before the flood year, and F_w =5.9 W m^{-2} after the flood year with an RMSE of 0.11 m, very similar to the 0.09 m reported by Obryk et al. (2016). Future simulations held the last F_w value until 2099. However, as mentioned before, in 2054 the mean summer air temperatures reached the historical unusual values of the flood year introduced by Gooseff et al. (2017). Hence, the sensible heat flux from the lake should increase to be consistent with our model formulation. Even when the F_w should increase in the future simulations, e.g., in 2054 that is thought as a new flood year, we kept this heat flux constant to avoid increasing the uncertainty of model results (recall that future climate projections intrinsically have an important uncertainty). Nevertheless, it is likely that an increase in F_w will lead to an important reduction of ice growth rates in autumn and winter. In consequence, the ice cover of WLB will thin faster than our predictions.

The incoming heat flux from the lake, combined with the conductive heat flux at the ice bottom, regulate the latent heat of freezing released to the atmosphere during periods of ice growth through ice conduction (Lepparanta, 2015), as shown in Equation (4.6). For each modeled case, the long-term period exhibited a significant increase in ice growth

rates of April and March (Figure 5.5c). The reason of this change is that the thinner the ice, the smaller the distance available for heat conduction. Thus, the larger the ice growth rate of the ice cover. Figure 6.1a shows the yearly average distribution of simulated F_{cb} for the three evaluation time periods. It can be seen that long-term F_{cb}, reached the value of F_w =5.9 W m^{-2} in the first days of March, contrary to the historical and mid-term simulations (mid March). Then, from April to mid September conductive heat flux at the ice bottom grew 17% in average (respect to mid-term simulations), under the median climate delta. Also, this effect is reflected in the March total ice thickness change rate results (Table 5.3), which in the long-term time period under each climate delta, the ice cover of WLB gained ice instead of losing it as the trend of other periods.

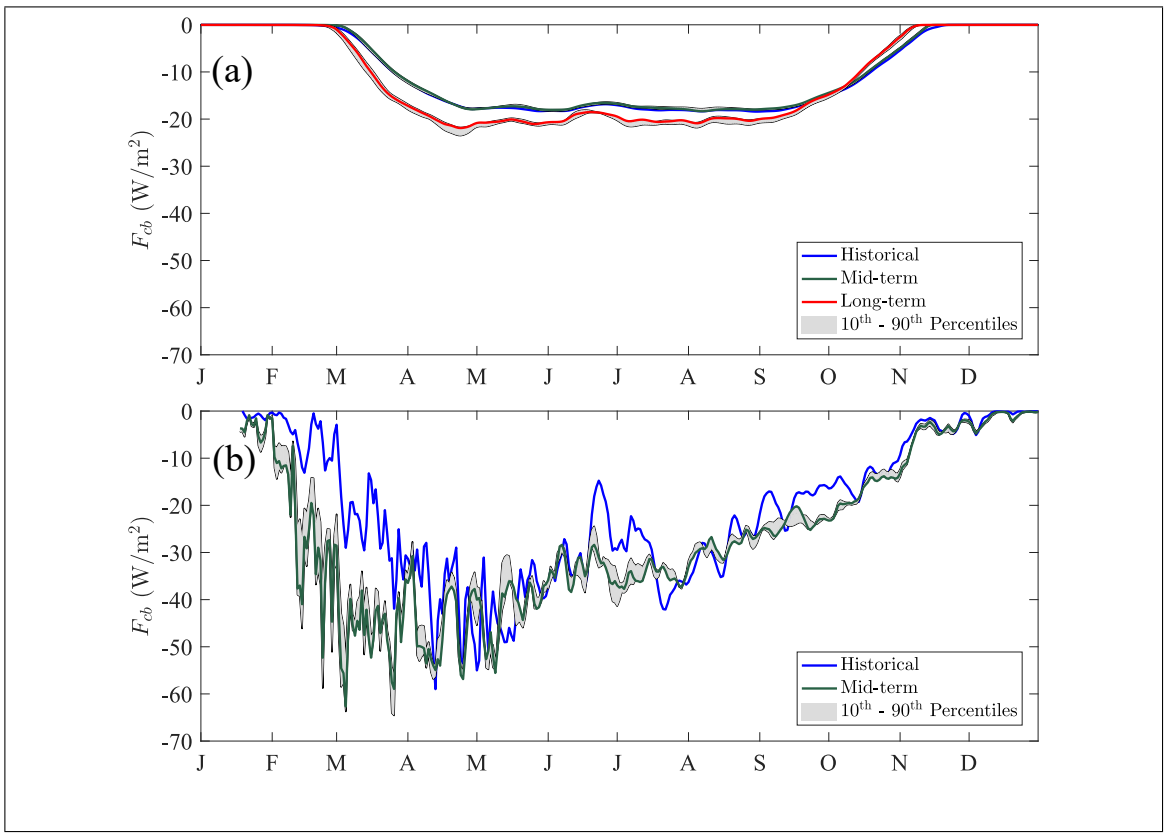

Figure 6.1. Yearly average of daily F_{cb} in: (a) WLB, and (b) Crooked Lake; for historical, mid-term, and long-term simulations, considering each hybrid climate delta. In Crooked Lake the results are shown since January 18th for comparison, due to the lack of data before that day in the historical time period. The difference between F_{cb} values of the ice covers from the two lakes, is an indicator of how distinct are their water thermal structures.

The increase of F_{cb} is clearly a modeling issue, closely related to the decision of maintaining F_w constant, which is the main limitation in this work. Studies in an Arctic lake showed that bottom melt is only relevant when the ice thins to $<$1 m (Dugan et al., 2013; Heron & Ming-Ko Woo, 1994), implying that in the ice cover of WLB the bottom melt rates should be negligible (Dugan et al., 2013). Therefore, in our model formulation for WLB, bottom melt may be augmented by numerical conditions (F_w used as a parameter). This is one of the reasons why our model validation in WLB presents a good fit with ice

thickness measurements (Figure 5.1b), but did not represent well the ablation measurements (Figure 5.2) with an RMSE of 0.28 m, against the 0.11 m calculated by Obryk et al. (2016). In this basis, ice thickness change rates found in this study should be considered as a total, and not individually (ice growth, ablation, bottom melt).

In Crooked Lake, February and March ice growth rates showed a great increase; whereas April and August ice growth rates decreased (Figure 5.7a, b) between the historical and the mid-term simulations. The bottom melt ceased in March. As in WLB, this particular changes were, most likely, due to the parametrization of F_w used in Crooked Lake. As indicated before, the linear regression established by Reid & Crout (2008) was considered to determine T_w and to calculate F_w. Nevertheless, the linear regression had an r^2 =0.69, being the lowest (July, August) and highest air temperatures (January, February) the values with the greatest dispersion respect to the linear tendency (see Fig. 11 of Reid & Crout (2008)). This shift is also appreciated in Table 5.4, in which the increment of total ice thickness change is noticeable, specially in February and March. It can be seen in Figure 6.1b, that between February and April the conductive heat flux at bottom increased, enhancing the ice growth.

Crooked Lake loses its ice cover under each hybrid climate delta simulated: (i) on the year 2064 for the 90$^{\text{th}}$ percentile climate delta, when mean summer and annual air temperatures are of -0.3 and -7.6 °C, respectively; (ii) on the year 2067 under the 10$^{\text{th}}$ percentile climate delta, when mean summer and annual air temperatures are of -0.1 and -8.3, respectively; and (iii) on the year 2069 under the 50$^{\text{th}}$ percentile climate delta, with mean summer and annual air temperatures of 0.1 and -7.5 °C, respectively. Will this ice cover come back? Our model did not consider ice formation in the complete absence of it. This is why the ice cover of Crooked Lake did not recover after it vanished. However, it is very likely that this lake will recover its ice cover in autumn or winter, exhibiting an ephemeral behavior. This behavior can be supported by analyzing the projected degree days above freezing, under each climate delta, as shown in Figure 6.2.

In the median projected simulation, before the ice melted completely in 2069, Crooked Lake experimented the austral summer (2068-2069) with more projected degree days (=87) above freezing (Figure 6.2b). Hence, more days of surface melting occurred, and maximum values of sensible and latent heat flux until that summer were observed: 248 and 62 W m^{-2}, respectively. For this reasons, the ice cover of Crooked Lake could not stop melting, until it disappeared in the first days of February. When the ice cover thickness reached values <0.2 m (mid January), it stopped being stable. Hence, other aspects of ice, such as mechanics and dynamics, should be taken into account (Lepparanta, 2015). Also, in some future years under every percentile climate delta the projected degree days above freezing are less than the summer when the ice vanished. Therefore, the ice cover of Crooked Lake may become perennial again. Nonetheless, under the median and 90^{th} percentile climate delta the ice cover would not exhibit a perennial behavior after 2079, while under the 10^{th} percentile climate delta the ice cover will be ephemeral after 2092. Note that the model implemented here corresponds to a spatial average, i.e., there were no considerations of the differences in the surface ice cover such as melt ponds, lateral melting, and ice ridges. Thus, it is likely that the ice cover of Crooked Lake melts in a great extension than that predicted in our analysis. On the other hand, at WLB (Figure 6.2a) the ice cover most likely will not melt this century because there are less projected degree days above freezing than those predicted at Crooked Lake.

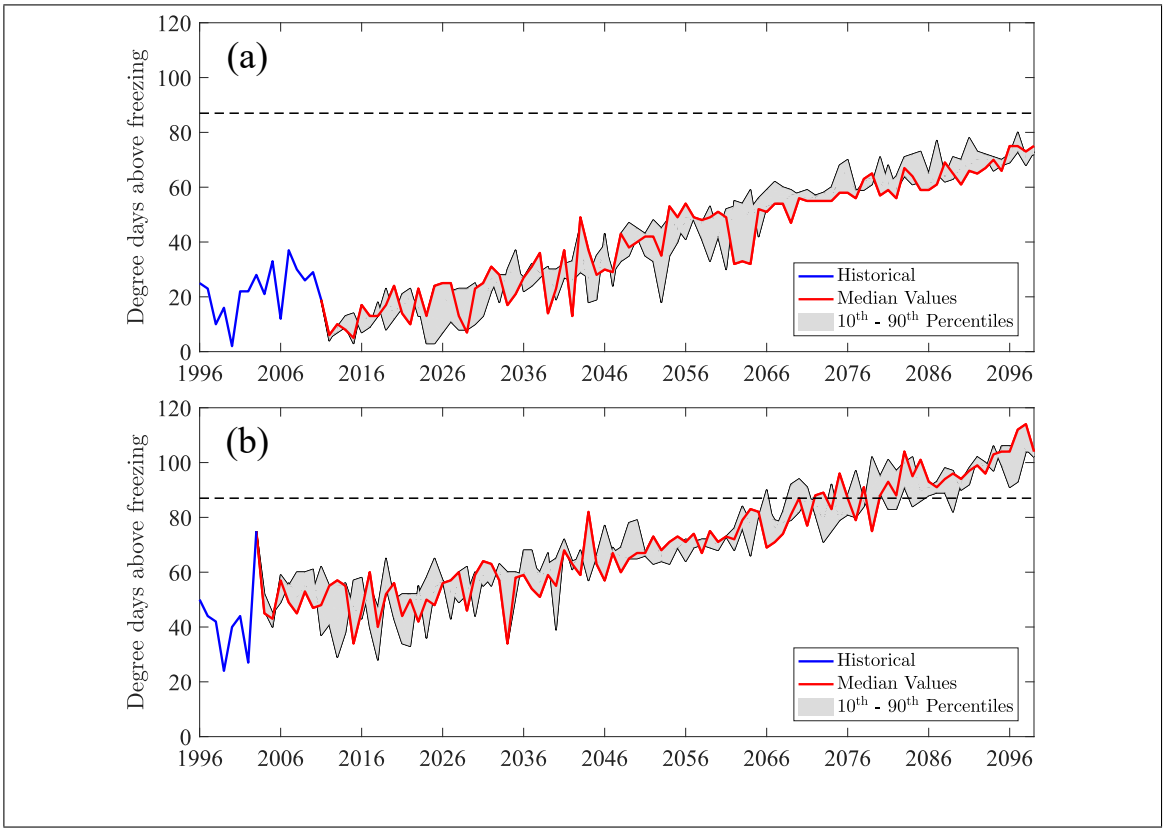

Figure 6.2. Historical and projected degree days above freezing for WLB (a) and Crooked Lake (b), under each hybrid climate delta. The dashed line indicates the limit between a perennial and a seasonal behavior of the ice cover (based on Crooked Lake projected results). Note that WLB did not reach the maximum projected degree days above freezing necessary to melt the ice cover of Crooked Lake.

The methodology employed in this study showed that using a one-dimensional ice-lake model combined with the hybrid delta approach can describe how Antarctic lakes will respond to climate change. Nonetheless, our estimates still have a relevant component of uncertainty. This uncertainty is associated with the lack of information regarding to the thermal structure of the lakes, the inherent uncertainty associated to the climate model projections, and the changes in interannual ice properties that are not taken into account (mainly the ice albedo that depends on the complex surface evolution of the ice, which still is a challenge in climate projections (Hohenegger, Alali, Steffen, Perovich, & Golden,

2012)). Therefore, the future projections presented in this work should be interpreted with caution.

7. CONCLUSIONS

An ice-lake model was developed to determine the ice thickness evolution of two Antarctic lakes: WLB and Crooked Lake; under three different future climate deltas determined by a hybrid delta approach. The model is forced by radiative fluxes, atmospheric turbulent fluxes, and a turbulent heat flux from the water body beneath the ice cover. The model solves the 1-D heat equation within the ice considering a set of moving boundary conditions. In this way, the model predicted the evolution of the ice cover thickness of each lake. We found that under the median climate delta, WLB will not lose its ice cover before 2100, and Crooked Lake will stop being perennial on 2079.

Even though the model validation in both lakes was satisfactory, future results should be interpreted with caution. As this work pointed out, ice-covered lakes respond to change in air temperatures, thinning their ice covers towards the future. However, this ice reduction was biased by the assumptions made to determine a turbulent heat flux from the lakes (constant flux in WLB, and a linear regression in Crooked lake), which caused an increase on ice growth rates. Therefore, the thermal structure of ice-covered lakes beneath their ice cover is a relevant physical feature that must be investigated if ice thickness evolution wants to be quantified over a long time period, as in a climate change analysis. Nonetheless, this work provides a first order analysis that can be used to comprehend the ice cover dynamics of these lakes, and recognize qualitatively how Antarctic ice-covered lakes will respond to a particular climate change scenario.

REFERENCES

Adrian, R., O'Reilly, C. M., Zagarese, H., Baines, S. B., Hessen, D. O., Keller, W., ... Winder, M. (2009). Lakes as sentinels of climate change. *Limnology and Oceanography*, *54*, 2283–2297.

Barnes-Keoghan, I. (2016). Antarctic Climate Data Collected by Australian Agencies. *Australian Antarctic Data Centre - CAASM Metadata*. Retrieved from `https://data.aad.gov.au/metadata/records/Antarctic{_}Meteorology`

Bennett, N. D., Croke, B. F., Guariso, G., Guillaume, J. H., Hamilton, S. H., Jakeman, A. J., ... Andreassian, V. (2013). Characterising performance of environmental models. In *Environmental modelling & software* (Vol. 40, pp. 1–20). Elsevier Ltd. doi: 10.1016/j.envsoft.2012.09.011

Benson, L. V., Lund, S. P., Burdett, J. W., Kashgarian, M., Rose, T. P., Smoot, J. P., & Schwartz, M. (1998). Correlation of late-Pleistocene lake level oscillations in Mono Lake, California, with North Atlantic climate events. *Quaternary Research*, *49*, 1–10.

Bitz, C. M., & Lipscomb, W. H. (1999). An energy-conserving thermodynamic model of sea ice. *Journal of Geophysical Research*, *104*(C7), 15669. doi: 10.1029/1999JC900100

Burke, C. M., & Burton, H. R. (1988). Photosynthetic bacteria in meromictic lakes and stratified fjords of the Vestfold Hills, Antarctica. *Hydrobiologia*, *165*, 13–23.

Castendyk, D. N., Obryk, M. K., Leidman, S. Z., Gooseff, M., & Hawes, I. (2016). Lake Vanda: A sentinel for climate change in the McMurdo Sound Region of Antarctica. *Global and Planetary Change*, *144*, 213–227. doi: 10.1016/j.gloplacha.2016.06.007

Cheng, B., & Launiainen, J. (1998). *A ONE-DIMENSIONAL THERMODYNAMIC AIR-ICE-WATER MODEL : TECHNICAL AND ALGORITHM DESCRIPTION REPORT* (Tech. Rep.). Helsinki, Finland: Finish Institue of Marine research.

Dana, G. L., Wharton Jr., R. A., & Dubayah, R. (1998). Solar radiation in the McMurdo Dry Valleys, Antarctic. In J. C. Priscu (Ed.), *Ecosystem dynamics in a polar desert: The mcmurdo dry valleys, antarctica. antarctic research series, vol. 72* (pp. 39–65).

Washington DC: American Geophysical Union.

Doran, P. T. (2014). McMurdo Dry Valleys Lakes Blue Box data (Continuous stage (lake level), ablation, surface PAR, underwater PAR). Enviromental Data Initiative.

Doran, P. T., Dana, G. L., Hastings, J. T., & Wharton, R. A. (1995). McMurdo Dry Valleys Long-Term Ecological Research (LTER): LTER automatic weather network (LAWN). *Antarctic Journal of the U.S.*, *30*(5), 276–280.

Doran, P. T., McKay, C. P., Clow, G. D., Dana, G. L., Fountain, A. G., Nylen, T., & Lyons, W. B. (2002). Valley floor climate observations from the McMurdo dry valleys, Antarctica, 1986-2000. *Journal of Geophysical Research Atmospheres*, *107*(24), 1–12. doi: 10.1029/2001JD002045

Dugan, H. A., Obryk, M. K., & Doran, P. T. (2013). Lake ice ablation rates from permanently ice-covered Antarctic lakes. *Journal of Glaciology*, *59*(215), 491–498. doi: 10.3189/2013JoG12J080

Fountain, A. G., Dana, G. L., Lewis, K. J., Vaughn, B. L., & McKnight, D. M. (1998). Glaciers of the McMurdo Dry Valleys, Southern Victoria Land, Antarctic. In J. C. Priscu (Ed.), *Ecosystem dynamics in a polar desert: The mcmurdo dry valleys, antarctica. antarctic research series, vol. 72* (pp. 65–76). Washington DC: American Geophysical Union.

Fountain, A. G., & Doran, P. T. (2014). Mcmurdo Dry Valleys Lake Bonney Meteorogical Station Measurements. Enviromental Data Initiative. Retrieved from `http://dx.doi.org/10.6073/pasta/f0f4fa889cfa725afb888caf7229f5bc`

Fountain, A. G., Lyons, W. B., Burkins, M. B., Dana, G. L., Peter, T., Lewis, K. J., ... Virginia, R. a. (1999). Physical Controls on the Taylor Valley Ecosystem, Antarctica. *BioScience*, *49*(12), 961–971.

Fountain, A. G., Nylen, T. H., Monaghan, A., Basagic, H. J., & Bromwich, D. (2010). Snow in the Mcmurdo Dry Valleys, Antarctica. *International Journal of Climatology*, *30*(5), 633–642. doi: 10.1002/joc.1933

Fritsen, C. H., & Priscu, J. C. (1999). Seasonal change in the optical properties of the

permanent ice cover on Lake Bonney, Antarctica: consequences for lake productivity and phytoplankton dynamics. *Limnology and Oceanography*, *44*(2), 447–454. doi: 10.4319/lo.1999.44.2.0447

Gallagher, J. B., Burton, H. R., & Calf, G. E. (1989). Meromixis in an Antarctic fjord: a precursor to meromictic lakes on an isostatically rising coastline. *Hydrobiologia*, *172*, 235–254.

Gettelman, A., Liu, X., Ghan, S. J., Morrison, H., Park, S., Conley, A. J., ... Li, J. L. F. (2010). Global simulations of ice nucleation and ice supersaturation with an improved cloud scheme in the Community Atmosphere Model. *Journal of Geophysical Research Atmospheres*. doi: 10.1029/2009JD013797

Gibson, J. A. E. (1999). The meromictic lakes and stratified marine basins of the Vestfold Hills, East Antarctica. *Antarctic Science*, *11*(02), 175–192. doi: 10.1017/S0954102099000243

Gooseff, M. N., Barrett, J. E., Adams, B. J., Doran, P. T., Fountain, A. G., Lyons, W. B., ... Wall, D. H. (2017). Decadal ecosystem response to an anomalous melt season in a polar desert in Antarctica. *Nature Ecology & Evolution*, *1*(September), 1334–1338. doi: 10.1038/s41559-017-0253-0

Goring, D. G., & Nikora, V. I. (2002). Despiking acoustic doppler velocimeter data. *Journal of Hydraulic Engineering*, *128*(1), 117–126.

Hausner, M. B., Wilson, K. P., Gaines, D. B., Suárez, F., Scoppettone, G. G., & Tyler, S. W. (2016). Projecting the effects of climate change and water management on Devils Hole pupfish (Cyprinodon diabolis) survival. *Ecohydrology*, *9*(4), 560–573. doi: 10.1002/eco.1656

Heron, R., & Ming-Ko Woo. (1994). Decay of a high Arctic lake-ice cover: observations and modelling. *Journal of Glaciology*, *40*(135), 283–292. doi: http://dx.doi.org/10.3198/1994JoG40-135-283-292

Hibler III, W. D. (1979). *A Dynamic Thermodynamic Sea Ice Model* (Vol. 9) (No. 4). doi: 10.1175/1520-0485(1979)009<0815:ADTSIM>2.0.CO;2

Hoare, R., Popplewell, K., House, D., Henderson, R., Prebble, W., & Wilson, A. (1964).

Lake Bonney, Taylor Valley, Antarctica: A Natural Solar Energy Trap. *Nature*, *202*, 693–694. doi: 10.1038/202886a0

Hoffmann, F., & Gardner, R. (1983). Evaluation of uncertainties in environmental radiological assessment models. In J. Till & H. Meyer (Eds.), *Radiological assessment: a textbook on environmental does assessment us nuclear regulatory commission.* Washington DC.

Hohenegger, C., Alali, B., Steffen, K. R., Perovich, D. K., & Golden, K. M. (2012). Transition in the fractal geometry of Arctic melt ponds. *Cryosphere*, *6*(5), 1157–1162. doi: 10.5194/tc-6-1157-2012

Holland, M. M., Bailey, D. A., Briegleb, B. P., Light, B., & Hunke, E. (2012). Improved sea ice shortwave radiation physics in CCSM4: The impact of melt ponds and aerosols on Arctic sea ice. *Journal of Climate*, *25*, 1413–1430.

Howard-williams, C., Schwarz, A.-m., Hawes, I., & Priscu, J. C. (1998). Optical Properties of the McMurdo Dry Valley Lakes, Antarctica. In *Ecosystem processes in a polar desert: The mcmurdo dry valleys, antarctica* (pp. 189–203).

Hunke, E. C., Lipscomb, W. H., Turner, A. K., Jeffery, N., & Elliot, S. (2015). *CICE : the Los Alamos Sea Ice Model Documentation and Software User's Manual.*

Hurrel, J. W., Holland, M. M., Gent, P. R., Ghan, S., Kay, J. E., Kushner, P. J., … Marshall, S. (2013). The Community Earth System Model: A Framework for Collaboratibe Research. *Bulletin of the American Meteorological Society*. doi: 10.1175/BAMS-D-12-00121.1

Jordan, R. E., Andreas, E. L., & Makshtas, A. P. (1999). Heat budget of snow-covered sea ice at North Pole 4. *Geophys. Res.-Oceans*, *104*, 7785–7806.

Kauffman, B. G., & Large, W. G. (2002). *The CCSM coupler, version 5.0.1. Technical note, National Center for Atmospheric Research* (Tech. Rep.).

Kay, J. E., Deser, C., Phillips, A., Mai, A., Hannay, C., Strand, G., … Vertenstein, M. (2015). The Community Earth System Model (CESM) Large Ensemble Project: A Community Resource for Studying Climate Change in the Presence of Internal Climate Variability. *Bulletin of the American Meteorological Society*, *96*, 1333–1349. doi:

10.1175/BAMS-D-13-00255.1

Kereyu, D., & Gofe, G. (2016). Convergence Rates of Finite Difference Schemes for the Diffusion Equation with Neumann Boundary Conditions. , *6*(2), 92–102. doi: 10.5923/j.ajcam.20160602.09

König-Langlo, G., & Augstein, E. (1994). *Parameterization of the downward long-wave radiation at the Earth's surface in polar regions* (Vol. 3).

LaBaugh, J. W., Winter, T. C., Rosenberry, D. O., Schuster, P. F., Reddy, M. M., & Aiken, G. R. (1997). Hydrological and chemical estimates of the water balance of a closed- basin in north central Minnesota. *Water Resources Research*, *33*, 2799–2812.

Laird, K. R., Fritz, S. C., Grimm, E. C., & Mueller, P. G. (1996). Century-scale paleoclimatic reconstruction from Moon Lake, a closed-basin lake in the northern Great Plains. *Limnology and Oceanography*, *41*(5), 890–902.

Launiainen, J., & Cheng, B. (1998). Modelling of ice thermodynamics in natural water bodies. *Cold Regions Science and Technology*, *27*(3), 153–178. doi: 10.1016/S0165-232X(98)00009-3

Launiainen, J., & Vihma, T. (1990). Derivation of turbulent surface fluxes: an iterative flux-profile method allowing arbitrary observing heights. *Environ. Software*, *5*, 113–124.

Lawrence, D. M., Oleson, K. W., Flanner, M. G., Thornton, P. E., Swenson, S. C., Lawrence, P. J., ... Slater, A. G. (2011). Parameterization improvements and functional and structural advances in Version 4 of the Community Land Model. *Journal of Advances in Modeling Earth Systems*. doi: 10.1029/2011MS00045

Laybourn-Parry, J., & Pearce, D. a. (2007). The biodiversity and ecology of Antarctic lakes: models for evolution. *Philosophical transactions of the Royal Society of London. Series B, Biological sciences*, *362*(1488), 2273–2289. doi: 10.1098/rstb.2006.1945

Legates, D. R., & McCabe Jr., G. J. (2005). Evaluating the Use of "Goodness of Fit" Measures in Hydrologic and Hydroclimatic Model Validation. *Water Resources Research*, *35*(1), 233–241. doi: 10.1029/1998WR900018

Lenaerts, J. T., Vizcaino, M., Fyke, J., van Kampenhout, L., & van den Broeke, M. R. (2016). Present-day and future Antarctic ice sheet climate and surface mass balance in

the Community Earth System Model. *Climate Dynamics*, *47*(5-6), 1367–1381. doi: 10.1007/s00382-015-2907-4

Lepparanta, M. (2015). *Freezing of Lakes and the Evolution of their Ice Cover*. Helsinki, Finland: Springer.

Lumley, J. L., & Panofsky, H. A. (1964). *The strucure of atmospheric turbulence*. New York: Wiley.

Lyons, W. B., Laybourn-Parry, J., Welch, K. A., & Priscu, J. C. (2006). Antarctic lake systems and climate change. In D. M. Bergstrom, P. Covey, & A. H. L. Huiskes (Eds.), *Trends in antarctic terrestrial and limnetic ecosystems* (pp. 273–295). Dordrecht, Netherlands: Springer.

Maykut, G. A., & McPhee, M. G. (1995). Solar Heating of the Arctic Mixed-Layer. *Journal of Geophysical Research*, *100*, 24691–24703. doi: 10.1029/95JC02554

Maykut, G. A., & Untersteiner, N. (1971). Some results from a time-dependent thermodynamic model of sea ice. *Journal of Geophysical Research*, *76*(6), 1550–1575. doi: 10.1029/JC076i006p01550

McKay, C. P., Clow, G. D., Wharton, R. A., & Squyres, S. W. (1985). Thickness of ice on perennially frozen lakes. *Nature*, *313*(6003), 561–562. doi: doi: 10.1038/313561a0

Meinshausen, M., Meinshausen, N., Hare, W., Raper, S. C. B., Frieler, K., Knutti, R., ... Allen, M. (2009). Greenhouse emission targets for limiting global warming to 2C. *Nature*, *458*, 1158–1163.

Monin, F. E., & Obukhov, A. M. (1954). Basic laws of turbulent mixing in the surface layer of the atmosphere. *Contrib. Geophys. Inst. Acad. Sci.*, *24*(151), 163–187.

Mori, N., Suzuki, T., & Kakuno, S. (2007). Noise of Acoustic Doppler Velocimeter Data in Bubbly Flows. *Journal of Engineering Mechanics*, *133*(1), 122–125. doi: 10.1061/(ASCE)0733-9399(2007)133:1(122)

Nash, J., & Sutcliffe, J. (1970). River flow forecasting through conceptual models part i - a discussion of principles. *Journal of Hidrology*, *10*(3), 282–290.

Obryk, M. K., Doran, P. T., Hicks, J. A., McKay, C. P., & Priscu, J. C. (2016). Modeling the thickness of perennial ice covers on stratified lakes of the Taylor Valley, Antarctica.

Journal of Glaciology, *62*(235), 825–834. doi: 10.1017/jog.2016.69

Oviatt, C. G. (1997). Lake Bonneville fluctuations and global climate change. *Geology*, *25*, 155–158.

Palethorpe, B., Hayes-Gill, B., Crowe, J., Sumner, M., Crout, N., Foster, M., ... Laybourn-Parry, J. (2004). Real-time physical data acquisition through a remote sensing platform on a polar lake. *Limnology and Oceanography-Methods*, *2*, 191–201. Retrieved from `isi:000227420000005` doi: 10.4319/lom.2004.2.191

Panofsky, H. A. (1963). Determination of stress from wind and temperature measurements. *Quarterly Journal of the Royal Meteorological Society*, *89*(379), 85–94.

Paquette, M., Fortier, D., Mueller, D. R., Sarrazzin, D., & Vincent, W. F. (2015). Rapid disappearance of perennial ice on Canada's most northern lake. *Geophysical Research Letters*, *42*, 1433–1440.

Priscu, J. C. (2014). McMurdo Dry Valleys Ice Thickness for Taylor Valley Lakes, Antarctica. Enviromental Data Initiative. Retrieved from `http://dx.doi.org/10.6073/pasta/757cc89de68a31cce2c8d97069a69e50`

Ragotzkie, A., & Likens, G. E. (1964). The heat balance of two Antarctic lakes. *Limnol. Oceanog.*, *9*, 412–425.

Reid, T., & Crout, N. (2008). A thermodynamic model of freshwater Antarctic lake ice. *Ecological Modelling*, *210*(3), 231–241. doi: 10.1016/j.ecolmodel.2007.07.029

Schindler, D. W. (2009). Lakes as sentinels and integrators for the effects of climate change on watersheds, airsheds, and landscapes. *Limnology and Oceanography*, *54*, 2349–2358.

Scott, R. F. (1905). *The Voyage of Discovery*. London: McMillan and Co.

Semtner, A. J. (1976). *A Model for the Thermodynamic Growth of Sea Ice in Numerical Investigations of Climate* (Vol. 6) (No. 3). doi: 10.1175/1520-0485(1976)006<0379:AMFTTG>2.0.CO;2

Smith, R. D. (1999). Marine ecosystem sensitivity to climate change. *BioScience*, *49*, 393–404.

Smith, R. D., Jones, P. W., Briegleb, B., Bryan, F., Danabasoglu, G., Dennis, J., ...

Others (2010). The Parallel Ocean Program (POP) reference manual: ocean component of the Community Climate System Model (CCSM). Los Alamos Natl Lab LAUR-10-01853.

Spigel, R. H., & Priscu, J. C. (1998). Physical Limnology of the Mcmurdo Dry Valleys Lakes. In J. C. Priscu (Ed.), *Ecosystem dynamics in a polar desert: The mcmurdo dry valleys, antarctica* (pp. 153–187). Washington DC: American Geophysical Union.

Stefan, J. (1891). Uber die Theorie der Eisbildung, insbesondere uber die Eisbildung im Polarmeere. *Annalen der Physik*, *278*(2), 269–286. doi: 10.1002/andp.18912780206

Tennekes, H., & Lumley, J. L. (1972). *A First Course in Turbulence*. MIT Press.

Vincent, A. C., Mueller, D. R., & Vincent, W. F. (2008). Simulated heat storage in a perennially ice-covered high Arctic lake: Sensitivity to climate change. *Journal of Geophysical Research*, *113*(C04036).

Vincent, W. F., Laurion, I., & Pienitz, R. (1998). Arctic and Antarctic lakes as optical indicators of global change. *Annals of Glaciology*, *27*, 691–696.

Wahl, T. L. (2003). Discussion of Despiking acoustic doppler velocimeter data'. *Journal of Hydraulic Engineering*, *129*(6), 484–488.

Wharton Jr., R. A., McKay, C. P., Clow, G. D., Andersen, D. T., Simmons, J. R. G. M., & Love, F. G. (1992). Changes in ice cover thickness and lake level of Lake Hoare, Antarctica: implications for local climatic change. *Journal of Geophysical Research*, *97*, 3503–3513.

Williamson, C. E., Saros, J. E., Vincent, W. F., & Smol, J. P. (2009). Lakes and reservoirs as sentinels, integrators, and regulators of climate change. Limnol. Oceanogr. 54, 22732282. Wilson, A.T., 1964. Evidence fromchemical diffusion of a climatic change in theMcMurdo Dry Valleys 1200 years ago. *Nature*, *201*, 176–177.

APPENDICES

A. LIST OF PARAMETERS

ρ_i	Density of ice (915 kg m^{-3})	T_a	Air temperature (°C)
ρ_a	Density of air (kg m^{-3})	T_{ak}	Air temperature (K)
ρ_w	Density of water (1000 kg m^{-3})	P_o	Standard atmospheric pressure (1013.25 hPa)
c_i	Specific heat capacity of ice (2.108·10^3 J kg^{-1} K^{-1})	R	Gas constant of dry air (287 J kg^{-1} K^{-1})
c_a	Specific heat capacity of air (1.004·10^3 J kg^{-1} K^{-1})	C_s	Bulk transfer coefficient (J kg^{-1} K^{-1})
c_w	Specific heat capacity of water (4.190·10^3 J kg^{-1} K^{-1})	C_l	Bulk transfer coefficient (J kg^{-1} K^{-1})
k_i	Thermal conductivity of ice (2.3 W m^{-1} deg^{-1})	C_w	Bulk transfer coefficient (J kg^{-1} K^{-1})
L_f	Latent heat of freezing (3.337·10^5 J kg^{-1})	q_a	Specific humidity of air (-)
L_s	Latent heat of sublimation (2.834·10^6 J kg^{-1})	q_s	Specific humidity of the surface (-)
L_e	Latent heat of vaporization (2.501·10^6 J kg^{-1})	RH	Relative humidity (%)
β	Absorption at surface (0.45)	ε	Vapour pressure (hPa)
κ	Extinction coefficient (0.85 m^{-1})	H	Total ice thickness (m)
α	Albedo (-)	z	Depth (m)
I	internal heat source (W m^{-2})	t	Time (s)
F_{sw}	Shortwave radiation (W m^{-2})	T_i	Ice temperature (°C)
$F_{lw\downarrow}$	Incoming longwave radiation (W m^{-2})	T_w	Water temperature (°C)
$F_{lw\uparrow}$	Outgoing longwave radiation (W m^{-2})	T_f	Freezing temperature of fresh water (273.15 K)
F_s	Sensible heat flux (W m^{-2})	u^*	Characteristic velocity scale (m s^{-1})
F_l	Latent heat flux (W m^{-2})	Q^*	Characteristic humidity scale (-)
F_{ct}	Conductive heat flux at surface (W m^{-2})	Θ^*	Characteristic temperature scale (°C)
F_{net}	Net surface heat flux (W m^{-2})	κ_v	von Kármán constant (0.4)
F_{cb}	Conductive heat flux at bottom (W m^{-2})	z_h	Vertical height (3 m)
F_w	Sensible heat flux from the lake (W m^{-2})	L	Monin-Obukhov length (m)
C	Cloud cover (0-1)	ϕ_m	Differential universal function (-)
S	Solar constant (1376 W m^{-2})	ϕ_h	Differential universal function (-)
Z	Zenith angle (rad)	z_o	Roughness length for momentum (5·10^{-4} m)
ϵ_i	Emissivity of ice (0.97)	z_q	Roughness length for humidity (5·10^{-4} m)
σ	Stefan-Boltzmann constant (5.67·10^{-7} W m^{-2} K^{-4})	z_T	Roughness length for temperature (5·10^{-4} m)
U_a	Wind speed (m s^{-1})	ψ_m	Integrated universal function (-)
U_w	Water speed (m s^{-1})	ψ_h	Integrated universal function (-)
dh/dt	Ice thickness change rate (cm month^{-1})	g	Acceleration of gravity (9.81 m s^{-2})
T_s	Surface temperature (°C)	Υ	Stability (-)
T_{sk}	Surface temperature (K)	χ	Stability function (-)
N	Number of ice layers (50)	z_{ref}	Reference height (10 m)
Δz	Ice layer thickness (m)	Δt	Time step (3 h)

B. FORMULAE FOR HEAT FLUXES

B.1. Fluxes at the top of the ice

B.1.1. Downwelling shortwave radiation flux (F_{sw})

Solar shortwave radiation was determined using the empirical equation proposed by Reid & Crout (2008):

$$F_{sw} = (1 - 0.48C)\, S cos Z\, (0.33 + 0.43 cos Z) \tag{B.1}$$

where C is the cloud fraction, S is the solar constant, and Z is the zenith angle (which depends on latitude, Julian day and solar time).

B.1.2. Upwelling longwave radiation flux ($F_{lw\uparrow}$)

The upwelling longwave radiation flux is calculated as in Launiainen & Cheng (1998):

$$F_{lw\uparrow} = -\epsilon_i \sigma T_{sk}^4 \tag{B.2}$$

where ϵ_i is the emissivity of ice, σ is the Stefan-Boltzmann constant, and T_{sk} is the surface temperature.

B.1.3. Downwelling longwave radiation flux ($F_{lw\downarrow}$)

The downwelling longwave radiation flux was parameterized by Konin-Langlo & Augstein (1994) for an Antarctic site (considering the effects of cloudiness and water vapor on atmospheric emissivity):

$$F_{lw\downarrow} = \left(0.765 + 0.22C^3\right)\sigma T_{ak}^4 \tag{B.3}$$

where T_{ak} is the air temperature.

B.1.4. Conductive heat flux at the ice surface (F_{ct})

The conductive heat flux at the ice surface is described by (Launiainen & Cheng, 1998):

$$F_{ct} = -k_i \left[\frac{\partial T_i}{\partial z} \right]_{z=0} \tag{B.4}$$

where k_i is the thermal conductivity of ice, T_i is the ice temperature and z is the depth. The temperature gradient is evaluated at $z = 0$; the surface of the ice cover.

B.1.5. Sensible heat flux (F_s)

The turbulent sensible heat flux is calculated as in Hunke et al. (2015):

$$F_s = \rho_a c_a C_s \left(T_a - T_s \right) U_a \tag{B.5}$$

where ρ_a is the air density, c_a is the heat capacity of air, C_s is a nonlinear bulk transfer coefficient determined by the Monin-Obukhov similarity theory (see Appendix C), and U_a is wind speed. The air density is calculated using the ideal gas law:

$$\rho_a = \frac{P_o}{R T_a} \tag{B.6}$$

where T_a is the air temperature, P_o is the standard atmospheric pressure, and R is the gas constant.

B.1.6. Latent heat flux (F_l)

The turbulent latent heat flux is calculated as in Hunke et al. (2015):

$$F_l = \rho_a L_{es} C_l \left(q_a - q_s \right) U_a \tag{B.7}$$

where L_{es} is the latent heat of vaporization (L_e) if ice is melting at the surface. Otherwise, it is the latent heat of sublimation (L_f). C_l is a nonlinear bulk transfer coefficient determined by the Monin-Obukhov similarity theory (see Appendix C). The specific humidity of air, q_a, and the specific humidity of the surface, q_s, are determined by (Launiainen &

Cheng, 1998):

$$q_a = \frac{0.622\varepsilon(T_{ak})RH}{P_o - 0.378\varepsilon(T_{ak})RH} \tag{B.8}$$

$$q_s = \frac{0.622\varepsilon(T_{sk})}{P_o - 0.378\varepsilon(T_{sk})} \tag{B.9}$$

where RH is relative humidity and ε is vapour pressure, which is defined as in Cheng & Launiainen (1998):

$$\varepsilon(T) = \begin{cases} exp\left(-\left(\frac{6763.6}{T}\right) - 4.9283ln\left(T\right) + 54.23\right) & if\ T \geq 273.15\ K \\ exp\left(-\left(\frac{6141}{T}\right) + 24.3\right) & if\ T < 273.15\ K \end{cases} \tag{B.10}$$

B.2. Fluxes at the ice bottom

B.2.1. Conductive heat flux at the ice bottom (F_{cb})

The conductive heat flux at the bottom of the ice is described by (Launiainen & Cheng, 1998):

$$F_{cb} = k_i \left[\frac{\partial T_i}{\partial z}\right]_{z=H} \tag{B.11}$$

in this case the temperature gradient is evaluated at $z = H$; the bottom of the ice cover.

B.2.2. Sensible heat flux from the lake (F_w)

If the turbulent heat flux between the lake and the ice cover is not taken as a constant, it is parameterized as in Maykut & McPhee (1995):

$$F_w = \rho_w c_w C_w \left(T_w - T_f\right) U_w \tag{B.12}$$

where ρ_w is the water density, c_w is the heat capacity of fresh water, C_w is a nonlinear bulk transfer coefficient, and U_w is water speed.

C. MONIN-OBUKHOV SIMILARITY THEORY

According to the Monin-Obukhov similarity theory (Monin & Obukhov, 1954; Lumley & Panofsky, 1964; Launiainen & Cheng, 1998), the dimensionless vertical gradients of velocity, specific humidity and temperature can be expressed as functions of their characteristic lengths, surface roughness and the Monin-Obukhov length (Launiainen & Vihma, 1990; Lepparanta, 2015):

$$\frac{\partial U_a}{\partial z} = \frac{u^*}{\kappa_v z_h}\phi_m\Big(\frac{z_h}{L}\Big) \tag{C.1}$$

$$\frac{\partial q_a}{\partial z} = \frac{Q^*}{\kappa_v z_h}\phi_h\Big(\frac{z_h}{L}\Big) \tag{C.2}$$

$$\frac{\partial T_a}{\partial z} = \frac{\Theta^*}{\kappa_v z_h}\phi_h\Big(\frac{z_h}{L}\Big) \tag{C.3}$$

where U_a is the wind speed magnitude, q_a is the specific humidity of air, T_a is the temperature of air, z_h is the vertical height, κ_v is the von Kármán constant, L is the Monin-Obukhov length; u^*, Q^* and Θ^* are the characteristic scales; and ϕ_m, ϕ_h are the differential universal functions of the boundary layer (Launiainen & Vihma, 1990). The integral forms of Equations (C.1), (C.2) and (C.3) are:

$$U_a = \frac{u^*}{\kappa_v}\left[log\left(\frac{z_h}{z_o}\right) - \Psi_m\Big(\frac{z_h}{L}\Big)\right] \tag{C.4}$$

$$q_a - q_s = \frac{Q^*}{\kappa_v}\left[log\left(\frac{z_h}{z_q}\right) - \Psi_h\Big(\frac{z_h}{L}\Big)\right] \tag{C.5}$$

$$T_a - T_s = \frac{\Theta^*}{\kappa_v}\left[log\left(\frac{z_h}{z_T}\right) - \Psi_h\Big(\frac{z_h}{L}\Big)\right] \tag{C.6}$$

where q_s is the surface specific humidity, T_s is the surface temperature, z_o is the roughness length for momentum, z_q is the roughness length for humidity and z_T is the roughness length for temperature. Ψ_m, Ψ_h are the integrated universal functions of the boundary

layer (Panofsky, 1963; Lepparanta, 2015). To calculate the sensible and latent heat fluxes, the bulk transfer coefficients of temperature and humidity are needed. Equations (B.5) and (B.7) are rewritten as (Tennekes & Lumley, 1972):

$$F_l = -\rho_a L_{es} Q^* u^* \tag{C.7}$$

$$F_s = -\rho_a c_a \Theta^* u^* \tag{C.8}$$

and combining them with Equations (C.4), (C.5) and (C.6), the bulk transfer coefficients can be obtained:

$$C_l = \frac{\kappa_v^2}{\left[log\left(\frac{z_h}{z_o}\right) - \Psi_m\left(\frac{z_h}{L}\right)\right]\left[log\left(\frac{z_h}{z_q}\right) - \Psi_h\left(\frac{z_h}{L}\right)\right]} \tag{C.9}$$

$$C_s = \frac{\kappa_v^2}{\left[log\left(\frac{z_h}{z_o}\right) - \Psi_m\left(\frac{z_h}{L}\right)\right]\left[log\left(\frac{z_h}{z_T}\right) - \Psi_h\left(\frac{z_h}{L}\right)\right]} \tag{C.10}$$

Equations (C.9) and (C.10) relates the bulk transfer coefficients with the stability of the atmospheric boundary layer ($\Upsilon = z_h/L$), defined by Hunke et al. (2015) as:

$$\Upsilon = \frac{\kappa_v g z_h}{u^{*2}}\left(\frac{\Theta^*}{T_a\left(1 + 0.606 q_a\right)} + \frac{0.606 Q^*}{1 + 0.606 q_a}\right) \tag{C.11}$$

where g is the acceleration of gravity. The above equation includes a correction due to the presence of moisture. Υ is restrained to have a magnitude less than 10.

Many empirical equations for the universal functions of the boundary layer are available in literature, both for the stable ($\Upsilon > 0$) and the unstable ($\Upsilon < 0$) cases. In the present work the approach of Kauffman & Large (2002) for the unstable case, and the approach

of Jordan et al. (1999) for the stable case are used:

$$\Psi_m = \begin{cases} -\left[0.7\Upsilon + 0.75\left(\Upsilon - 14.3\right) exp\left(-0.35\Upsilon\right) + 10.7\right] & if\ \ \Upsilon > 0 \\ 2ln\left[0.5\left(1+\chi\right)\right] + ln\left[0.5\left(1+\chi^2\right)\right] - 2arctan\left(\chi\right) + \dfrac{\pi}{2} & if\ \ \Upsilon < 0 \end{cases} \tag{C.12}$$

$$\Psi_h = \begin{cases} -\left[0.7\Upsilon + 0.75\left(\Upsilon - 14.3\right) exp\left(-0.35\Upsilon\right) + 10.7\right] & if\ \ \Upsilon > 0 \\ 2ln\left[0.5\left(1+\chi^2\right)\right] & if\ \ \Upsilon < 0 \end{cases} \tag{C.13}$$

where $\chi = \left(1 - 16\Upsilon\right)^{0.25}$.

Equations (C.9)-(C.13) form a non-linear system (Monin-Obukhov boundary layer equations), which is solved iteratively, using the Kauffman & Large (2002) method, to determine C_s and C_l. In this procedure it is assumed that $z_o \approx z_T \approx z_q$.

D. MODEL ALGORITHM

In this section, the algorithm of the model employed in this work, including its principal features and discretizations, is described. First, Equation (4.1) is discretized using the BTCS method:

$$\rho_i c_i \frac{\left(T_k^{m+1} - T_k^m\right)}{\Delta t} = k_i^* \frac{\left(T_{k-1}^{m+1} - 2T_k^{m+1} + T_{k+1}^{m+1}\right)}{2\Delta z} - \beta F_{sw} \frac{exp^{-\kappa(k-1)\Delta z} - exp^{-\kappa(k)\Delta z}}{\Delta z} \tag{D.1}$$

where k is a space index, m is a time index, Δt is the time step, Δz is the thickness of one ice layer and k_i^* is the thermal conductivity of ice equals to k_{ice} except at borders where is equals to $2k_{ice}$. The above equation is solved using a tridiagonal matrix method, which form is:

$$-\xi T_{k-1}^{m+1} + \left(1 + 2\xi\right) T_k^{m+1} - \xi T_{k+1}^{m+1} = T_k^m + \xi\left(exp^{-\kappa(k-1)\Delta z} - exp^{-\kappa(k)\Delta z}\right) \tag{D.2}$$

where $\xi = k_i^* \Delta t / (\rho_i c_i \Delta z)$.

To solve (D.2), initial and boundary conditions are needed. As mentioned in the text, it is assumed that the initial temperature profile within the ice is a constant gradient between the temperature of the air, at the beginning of the simulation, and T_f (fixed bottom boundary condition):

$$T_k^0 = \left(\frac{T_f - T_a^0}{N}\right) \cdot \left(\frac{2k-1}{2}\right) + T_a^0 \tag{D.3}$$

where N is the number of layers. The top boundary condition is the surface ice temperature, T_s, calculated using Equation (4.3), which is nonlinear. F_{sw} and $F_{lw\downarrow}$ are directly computed with the input data using Equations (B.1) and (B.3), respectively; $F_{lw\uparrow}$, F_s, F_l and F_{ct} are functions of T_s so they cannot be known. For the calculation of the turbulent fluxes, the iterative method proposed by Kauffman & Large (2002) is used. At the beginning of the iterations, Equations (C.4), (C.5) and (C.6) are rewritten as:

$$u^* = c_u U_a \tag{D.4}$$

$$Q^* = c_q \left(q_a - q_s\right) \tag{D.5}$$

$$\Theta^* = c_\theta \left(T_a - T_s\right) \tag{D.6}$$

where c_u, c_q and c_θ are initialized as:

$$\frac{\kappa_v}{ln\left(\frac{z_{ref}}{z_o}\right)} \tag{D.7}$$

where z_{ref} is a reference height set to 10 m.

Then the stability parameter is computed using Equation (C.11), and the turbulent scales are obtained. With the value of Υ, the stability criterion is applied (stable or unstable case) and the universal integrated function is chosen between Equations (C.12) and (C.13).

After this, the coefficients from Equations (D.4), (D.5) and (D.6) are updated:

$$\tilde{c_u} = \frac{c_u}{1 + \frac{c_u}{\kappa_v}\left(ln\left(\frac{z_h}{z_{ref}}\right) - \Psi_m\right)} \tag{D.8}$$

$$\tilde{c_q} = \frac{c_q}{1 + \frac{c_q}{\kappa_v}\left(ln\left(\frac{z_h}{z_{ref}}\right) - \Psi_h\right)} \tag{D.9}$$

$$\tilde{c_\theta} = \frac{c_\theta}{1 + \frac{c_\theta}{\kappa_v}\left(ln\left(\frac{z_h}{z_{ref}}\right) - \Psi_h\right)} \tag{D.10}$$

The iteration is finished with new turbulent scales. After a few iterations (more than four) the bulk transfer coefficients can be calculated:

$$C_s = \tilde{c_u}\tilde{c_\theta} \tag{D.11}$$

$$C_l = \tilde{c_u}\tilde{c_q} \tag{D.12}$$

Having these values, Equation (4.3) is solved with a linear approximation method (Equation (D.13)) specified by Hunke et al. (2015). In this way, an iterative loop is implemented to update the temperatures within the ice, checking that the following convergence criteria are met:

1) $T_s \leq 0°$.

2) The change in T_s between successive iterations is less than 0.0005°C.

3) $F_{net} \geq F_{ct}$. Otherwise ice will grow at the surface, which is not permitted.

$$F^*_{net} + \left(\frac{dF_{net}}{dT_s}\right)^* \left(T_s^{m+1} - T_s^*\right) = \frac{2k_i}{\Delta z}\left(T_s^{m+1} - T_1^{m+1}\right) \tag{D.13}$$

where T_s^* is the surface temperature of the ice from the most recent iteration, F^*_{net} and $(dF_{net}/T_s)^*$ are functions of T_s^*. Rearranging terms of Equation (D.13):

$$\left[\left(\frac{dF_{net}}{dT_s}\right)^* - \frac{2k_i}{\Delta z}\right] T_s^{m+1} + \frac{2k_i}{\Delta z} T_1^{m+1} = \left(\frac{dF_{net}}{dT_s}\right)^* T_s^* - F_{net}^* \tag{D.14}$$

The above equation is then coupled to Equation (D.2) as the first row of the tridiagonal system. At this point the heat equation is solved, and a new temperature profile is obtained. If at the end of the convergence iterations a temperature greater than $0°C$ exists within the ice, it is brought to $0°C$ by melting ice of the corresponding layer.

Finally, the new ice thickness must be found. The ice melts at the top surface if $F_{net} \geq F_{ct}$ as shown in Equation (4.4). If the top layer melts completely, the remaining energy is used for the rest of the ice layers. Also, at the top surface sublimation of ice can occur according Equation (4.5). The melting and sublimation rates are discretized as:

$$\left[\frac{dh}{dt}\right]_{z=0} = \frac{h_0^{m+1} - h_0^m}{\Delta t} \tag{D.15}$$

At the ice bottom, ice can grow or melt, depending on F_{cb} and F_w (see Equation (4.6)). The discretization of the growth or melt rate is:

$$\left[\frac{dh}{dt}\right]_{z=H} = \frac{h_{N+1}^{m+1} - h_{N+1}^m}{\Delta t} \tag{D.16}$$

and the discretization of the conductive heat flux at the ice bottom is:

$$F_{cb} = 2k_i \frac{\left(T_N^{m+1} - T_f^{m+1}\right)}{\Delta z} \tag{D.17}$$

At last, the ice layer thickness must be updated to keep a uniform spatial discretization, because the actual Δz varies for each layer after the ice cover has grow or melt. This is simply done by dividing the new total ice thickness H in the number of layers, but this process must ensure conservation of energy. To do this, the overlap, η_{kp}, is calculated between each new layer k and each old layer p as in Hunke et al. (2015):

$$\eta_{kp} = min\left(z_p, z_k\right) - max\left(z_{p-1}, z_{k-1}\right) \tag{D.18}$$

where z_k is the vertical coordinate of the new layer, and z_p is the vertical coordinate of the old layer. The conservation of energy is achieved updating the enthalpies of each layer:

$$q_k = \frac{1}{\Delta z} \sum_{p=1}^{N} \eta_{kp} q_p \tag{D.19}$$

the old enthalpy (energy required to melt an ice unit) is given by:

$$q_m = -\rho_i \left(-c_i T_m^{m+1} + L_s \right) \tag{D.20}$$

E. FLOWCHART OF THE MODEL RESOLUTION